UNIVERSITY OF READING
School of Mathematics, Meteorology and Physics

Convective Clusters and Self-Aggregation in Idealized High-Resolution Models: The role of Interactive Radiation

Francis Colledge
August 2010

A dissertation submitted in partial fulfilment of the requirement for the degree of MSc Applied Meteorology

Abstract

Several idealized modelling studies using Cloud-Resolving Models, have demonstrated the ability to form aggregated cloud clusters, whether they are large or small scale, in Radiative Convective Equilibrium. This aggregation has been observed in domains over 500km, including in recent runs of the UK Met Office idealized atmospheric model. These studies have indicated the conditions needed for self-aggregation to occur, including; small vertical wind shear of the horizontal wind, interaction of radiation with clouds and/or water vapour, and the effect of convectively enhanced surface winds on surface fluxes.

Convective organization has a high level of importance to many phenomena in tropical meteorology, and global weather and climate models have the inability to correctly predict. This study is a idealized modelling study investigating the role interactive radiation schemes has on the forming of aggregation.

Three different model datasets were investigated from the NERC funded CASCADE consortium project, created using the Met Office Unified Model (METUM). For all three experiments the SST was fixed at 300K, the lateral boundary conditions were cyclic, and with no imposed Coriolis forcing. One of the cases (NORAD) with 4km gird spacing had an imposed fixed radiative forcing in space and time. The other two datasets had interactive radiation schemes, with 4km grid spacing (HIGHRES), and 40km grid spacing (NORAD).

The NORAD experiment was unable to reach an equilibrium state and produce organized convection, the LOWRES was observed to start to reach a level of equilibrium with large-scale aggregation occurring. The HIGHRES reaching the equilibrium state by day 50, with related bands of organized convection across the top of the model domain.

The radiation interaction generated a low level circulation by mass continuity, as observed by Bretherton *et al.* (2005), which acted to feed the aggregation. The dry columns were associated with strong longwave cooling, which triggered a subsidence profile within the boundary layer and bottom level of the free troposphere.

Acknowledgements

Firstly, I would like to say thank you to my supervisors Dr Robert Plant and Dr Christopher E. Holloway for their enthusiasm and guidance throughout, enabling me to complete this project.

I would also like to pay a special thanks to my parents for providing the support and financial backing for this year, enabling me to pursue my dream and future career as a specialist in meteorology in the yacht racing industry.

Contents

List of figures

List of tables

Chapter 1 – Tropical Convection and Self-Aggregation

1.1 Introduction

Cloud and precipitation are very important features of the tropical atmosphere, because of that fact they are important for numerical weather prediction (NWP) and climate models, to predict correctly. The amount, height and thickness of cloud cover play an important part in governing the air temperature through interactions with radiation. This chapter introduces the role of convection in the tropics, discusses self-aggregation in the tropics, how convection is modelled, previous modelling studies of aggregation, and the project aim.

1.1.1 Tropical convections role in the global atmosphere

Hasternrath (1985) stated that 'The functioning of the global climate system can be understood only upon proper appreciation of processes in the tropics'. Hence a better understanding of tropical processes is needed to improve the skill of our weather forecasting and climate models.

In general the tropical climate is a climatic zone geographically between the Tropics of Capricorn and Cancer (23°N to 23°S). Within this region the incoming solar radiation is far greater than the outgoing terrestrial radiation, and the diurnal temperature cycle is greater than the annual temperature cycle. Therefore the net effect is that the tropics are heated; when equilibrium occurs, heat is exported by tropical weather systems to the extra-tropical region. The solar heating at the surface is transported into the atmosphere via surface fluxes, which is dominated by latent heat flux in the tropics. This latent heat is released in clouds, and the water returns to the surface as precipitation. The tropics are associated with high levels of precipitation/water vapour.

The Tropics are approximately in a convective-radiative quasi-equilibrium, and deep convection plays a crucial role in this (Grabowski and Petch, 2009). The quasi-equilibrium theory was originally proposed by Arakawa and Schubert (1974), and it is based on a statistical equilibrium between convection and large scale forcing such as radiation. The convective activity (stabilising the atmosphere) balances destabilisation (CAPE production) by large scale processes. The key assumption for this quasi-equilibrium is that the time scales of convection are fast compared to the timescale on which the large scale forcing acts to change the environment.

To remove the large-scale dynamics (such as the Hadley or Walker cells), the atmosphere is thought to be in Radiative Convective Equilibrium (RCE). In such an atmosphere, radiation together with surface enthalpy fluxes and convection act to destabilize the troposphere to moist convection (Emanuel and Khairoutdinov, 2010). The atmosphere would tend to approach radiative equilibrium (RE) after a period of time, which is where the emission of infrared radiation by each sample of air is exactly balanced by its absorption of infrared and shortwave radiation (Emanuel, 1994).

Understanding the role of deep convection in the atmospheric climate system, as well as future predictions of climate change, requires stringent modelling techniques across the micro scale up to the global scale using different models. Traditional circulation models are not able to represent deep convection with a high level of skill, and there is high uncertainty in how it may change in the perturbed climate (Grabowski and Petch, 2009).

Deep convection is an important source of mid to upper levels of tropospheric water vapour and high clouds which strongly affects the radiation budget of the earth. In the topics, high level clouds contain mixtures of ice and liquid water which in turn affects the transfer of short and long wave radiation has an impact varying the radiative heating gradients through the atmosphere (Yuan and Houze, 2010).

1.1.2 Observed Self-aggregation in the Tropics

Much of the convection in the tropics is organised and not random. This organisation occurs on a wide range of space and time scales. Convection is a response of the atmosphere to destabilization by column processes such as surface enthalpy fluxes and radiative cooling, and also by large scale circulation of atmosphere and associated enthalpy transport (Khairoutdinov and Emanuel, 2010).

Most types of moist convection are on a small scale of around a few kilometres in horizontal dimension (Byers and Braham, 1948; Malkus, 1954). These often merge into clusters of approximately 10km in horizontal dimension. Under certain environments convection becomes organised on larger scales.

Sheared environments provide conditions for various types of organised convective systems, for example; Squall lines, Mesoscale Convective Systems (MCS) and Superclusters. These forms of convective organization will be discussed within this section of the report in that particular order.

In the topics squall lines may form spontaneously or develop on arc segments of expanding, initially circular pools of cold air flowing outward near the surface from an isolated convective cell (Emanuel, 1994). The favourite environmental conditions that favour squall lines forming were stated by Zipser (2003), that empirically and theoretically the determining factor is the low level wind shear.

The most common type of squall line has a trailing stratiform precipitation region and a leading convective region ahead. The convective region is usually 10 to 30km in horizontal dimension ahead of the stratiform precipitation region that often exceeds 100km in horizontal dimension (Zisper, 2003). Although lines consisting of convective cells can be in the order of a few hundred km in length some may exceed lengths of 1000km.

In the tropics a large percentage of the rainfall is due to cloud clusters and MCSs, and Emanuel (1994) states that the 'physical characterisation remains an outstanding problem in meteorology'. MCS structures are sometimes formed of cumulonimbus clouds, and through which their anvils merge into a single mesoscale cirriform cloud shield (Houze, 1993). The anvils themselves may be at temperatures between -50 to -100°C. Oceanic anvils have been observed in the tropics to be more likely extending outward from large stratiform precipitation areas of MCSs, as opposed to being vertically aligned over the MCSs over continental regions such as West Africa (Cetrone and Houze, 2009).

MCS Clusters tend to form in environments with less wind shear than squall lines and MCSs often favour regions of large scale ascent. Figure 1.1 displays MCS clusters within a Supercluster, taken from the TOGA COARE project.

There are complex interactions between updrafts and downdrafts maintaining the system, and which also act to generate new cells. The MCSs activity often peaks at night, where convection is triggered in the early evening, which allows it to continue into the evening. The total system precipitation is proportional to the lifetime of the cluster, which may be as short as a few hours or as long as several days.

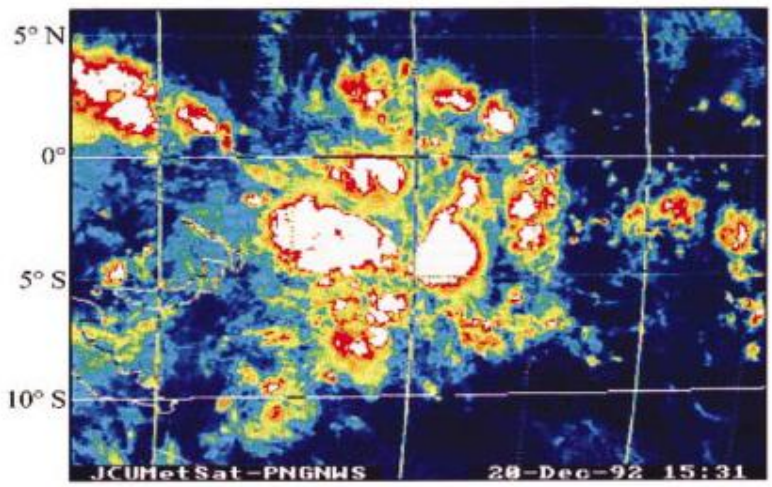

Figure 1.1 Mesoscale convective clusters embedded within a Supercluster, observed from space on 20th December 2003 during TOGA COARE. Mesoscale systems as white (cold) cloud tops observed by a geostationary satellite. (Source: Moncrieff, 2003, pp 1526)

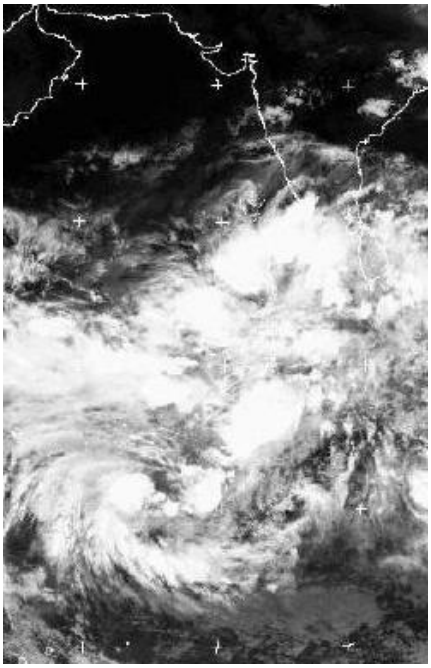

Figure 1.2 Supercluster over the Indian Ocean, with Tropical cyclone formation in the bottom left hand corner of the Infrared satellite image. May 2nd 2002, 1800 UTC (Source: MTMG19 Tropical Convection Module).

The term Supercluster was first used by Nakazawa (1988) to describe large regions of organized tropical convection, with diameters of the order 1000km and lifetimes generally more than 2 days. They can act as triggers for tropical cyclone formation as seen in figure 1.2 in the bottom left hand corner.

These Supercluster systems include the Madden-Julian Oscillation (MJO), discovered by Madden and Julian (1972). This feature is also known as the 40-60 day Intraseasonal Oscillation, during which active convection is observed that propagates eastwards, and leaves behind relatively suppressed conditions. The MJO has strong impacts such as; the Indonesian floods 2007-2008, Interactions with the Indian Monsoon to trigger active and break phases, strong modulation of tropical cyclone formation, and also has impacts on the US/Canada west coast precipitation.

1.2 Modelling convection in the tropics

The current limitations of NWP models and climate models ability to represent large-scale organised convective systems in the tropics has a great effect on their representation of the damage/impacts which occurs, as discussed in section 1.1.2 with the MJO and other systems. It is also said that the MJO may have an impact on the initiation and amplification of El Nino (Madden and Julian 1994; McPhaden 1999). The lack of forecasting skill also has an impact on other types of weather phenomena which are generated by mesoscale clusters and superclusters, such as tropical cyclones. The large scale atmospheric circulation is influenced by the degree and accuracy to which organized convection is predicted too.

The inability of models to simulate the MJO is thought to be related to their poor ability to represent cumulus convection generally (Waliser *et al.*, 2009). The MJO simulations have shown particular sensitivity related to the convective parameterization, or related processes such as cloud-radiative feedbacks (e.g., Slingo *et al.* 1996; Wang and Schlesinger 1999; Lee *et al.* 2001; Maloney and Hartmann 2001; Maloney 2002; Lee *et al.* 2003; cited by Waliser *et al.*, 2009).

To be able to understand these complex clusters and how they are formed, a simplified modelling technique has been used to try and replicate some of the main features of the tropical atmosphere. As stated in the section 1.1.1 convection can be viewed as being in quasi-equilibrium. To model the convection, the equilibrium is considered in its simplest form, RCE where Emanuel and Khairoutdinov (2010) state that ‘the effects of large-scale circulation on convection are ignored and only radiation, convection, and surface enthalpy fluxes are allowed to transfer energy.’

1.2.1 Parameterization

Convection occurs on too small a scale to be resolved by the relatively large grid spacing's that are normally used in NWP and climate models. A model can resolve reasonably well features that are approximately five times the size of the grid spacing. Parameterization is the process in which the effect of a subgrid process is expressed in terms of resolved model variables (ECMWF, 2007). It can either be statistical and physical, or even a combination of the both. For example models are heavily parameterised for convection on the grid scale of 40km as compared to 4km. This has an impact on the models ability to develop self aggregation clusters as observed in the topical environment, as they are mostly resolving the large scale convection and not the small scale individual cumulus clouds.

There are a variety of different cloud microphysics parameterization schemes that are used in models, with many having at least three different ice phase categories; cloud ice, snow, and graupel. This is necessary as different hydrometeors will have different terminal velocities, which will affect the different fall out speeds, the life time of the cloud, heating, precipitation rates, and radiative properties.

There are also a number of other parameterization schemes involved in models including, radiation schemes (which affect the models ability to react with different types of microphysics in the model), surface layer schemes (which calculate surface heat fluxes) and boundary layer schemes (which represent turbulence and other boundary layer processes). The convective scheme is required to determine the amount and lifetime of convection and the triggering function. The convective triggering function is a set of algorithms for determining the location and timing of sub-grid scale convection.

The parameterization schemes and model setup implemented by the model simulations in this investigation, is discussed later in Chapter 2, model and model setup.

1.3 Idealized Model Studies – Self-Aggregation

Cloud-resolving models (CRM) are numerical models which are able to resolve cloud-scale (and mesoscale) circulations in either two or three dimensions. CRMs have demonstrated to be capable of simulating convective-radiative responses to an imposed large-scale forcing. The cloud and radiative properties produced by CRMs have been studied to investigate the convective related processes and their multiple effects on large-scale circulations (Wu and Li,

2008). For a comprehensive review of cloud-resolving model studies of convective processes please read further the study by Wu and Li (2008).

There have been previous CRM studies where the effects of a parameterized radiation scheme were switched off, which were replaced by a simple cooling of the troposphere at a fixed rate in space and time. Cohen and Craig (2006) carried out a number of simulations with different radiative cooling rates, with imposed weak and strong vertical wind shears to produce different degrees of convective organization. The sea surface temperature (SST) was set at a uniform rate of 300K, and the atmosphere was assumed to be non-rotating. With no vertical wind shear, some spatial clustering of convective cells on a scale of 10-20km with lower forcings (-2 and -4 $Kday^{-1}$), it was found with large forcings (-8, -12, and -16$Kday^{-1}$), that similar scaled convective cells were observed with a tendency towards spatial regularity (Cohen and Craig, 2006).

Tompkins and Craig (1998a) aimed to evaluate the radiative convective interactions to gain a better understanding of the tropical climate. To address this a cloud-resolving model (CRM) was run to a radiative-convective equilibrium (RCE) state in three dimensions. The model included a three-phase bulk microphysical scheme and a fully interactive two-stream broadband radiative transfer scheme as described by Edwards and Slingo (1996), for the short wave and long wave radiation. Two time scales were clearly indicated by the model with the approach towards equilibrium, a short cumulus lifecycle of a few hours associated with individual events and a longer time-scale of around 30 days. The convection produced by the model was found to become organized in a band structure associated with high boundary layer moisture values. It was stated by Tompkins and Craig (1998a) that the self aggregation occurs because of the interaction of higher winds associated with convective horizontal mass convergence/divergence, and the wind sensitive surface fluxes. These authors also showed that interactive-radiation acts to localise convection (horizontally imposed homogeneous radiative heating rates acted to destroy aggregation after four days).

Bretherton *et al.* (2005) investigated the spatial organization of deep moist convection in radiative equilibrium over a constant sea surface temperature. A three-dimensional CRM over a 576km^2 domain was implemented with no ambient rotation and no mean wind for a 100 day simulation. In agreement with Tompkins and Craig (1998a), it was found that both cloud-radiation feedbacks and convective gustiness help to initiate self-aggregation. However, in this larger domain, the organization was into a cluster rather than bands. The self-aggregation

was based on convection forming in regions with a moist mid-troposphere. It was stated that as other regions started to dry out, they started to radiatively cool more strongly in the lower troposphere than the upper, and therefore bottom heavy radiative cooling had to be compensated by a bottom heavy subsidence profile. To drive this subsidence, a return flow from moist to dry regions in the lower to mid-troposphere developed above the boundary layer flow from dry to moist regions, which acted to amplify the self-aggregation by exporting moist static energy out of the dry regions increasing the amount of drying out in these regions. This produced a single small cluster in the domain, as displayed in figure 1.3, which shows precipitation (P) per day, Thermal Heat Flux (Latent plus sensible) (THF), water vapour path (WVP), and outgoing longwave radiation (OLR) . This low level circulation was found to resemble the cross-equatorial flow in the East and central Pacific.

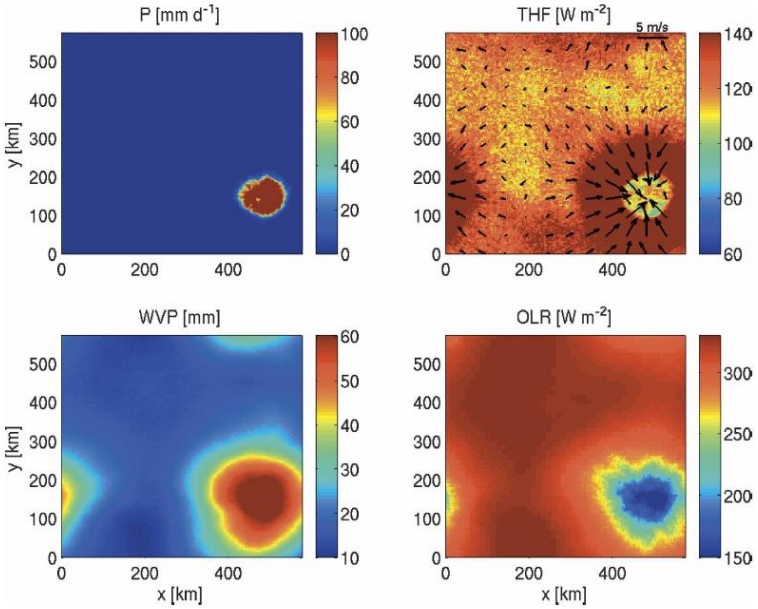

Figure 1.3 Horizontal maps of daily-mean P, THF with superimposed surface wind vector, WVP and OLR for day 50.
(Source: Bretherton *et al.*, 2005, pp4278)

Bretherton *et al.* (2005, pp4291) highlighted the importance 'of the interconnected vertical profiles of convection, vertical motion, and humidity in determining the exchange of moist static energy between moister and drier regions'. This was due to the advective moist static energy fluxes being extremely complex. However, an important conclusion is that feedbacks between convection and radiation and surface fluxes are needed to initiate self aggregation; changes to the microphysical scheme can also affect the self-aggregation, by modifying the

scale and lifetime of cirrus cloud, which has an impact on the column radiative cooling and moisture content.

Stephens *et al.* (2007) conducted experiments using both 2D and 3D versions of a CRM to examine the feedbacks between the radiative heating of clouds and convection. The equilibria found in the 2D and 3D experiments were quantitatively different, but qualitatively the feedbacks related to the radiative processes were found to be similar. The moist regions were found to be fed by the dry regions where most of the low level moistening was found to occur, and by conservation of mass broad-scale subsidence was found in the dry regions to compensate the upward motions in the convective regions. A number of experiments were run with the following different radiation assumptions; fully interactive, fixed (time and space), interactive without contributions by clouds and precipitation, and interactive without contributions from any clouds below 8km. From these experiments it was argued that there are two important mechanisms which govern equilibrium and the convection that forms within it. Firstly the gradients of radiative heating which are determined by cloud differences between wet and dry regions, which establish two differing contrasting modes of the moist equilibrium. Stephens *et al.* (2007) believed that the gradients were established by the high clouds of the moist regions. Secondly, once again, the radiative heating gradients are importantly set by the amount of high cloud detrained from convection. The experiments were able to show that high cloud radiative heating, which is an actual by-product of the convection, acts as a feedback to determine the amount of high cloud in moist regions.

Nolan *et al.* (2007) wanted to evaluate the relationship between the likelihood of tropical cyclogenesis and external environmental forcings by implementing a simple idealized model which was run to RCE on a doubly periodic f-plane. The control of the environment was reduced to three parameters; SST, the Coriolis parameter, and an imposed background surface wind. From these experiments it was concluded that unsheared RCE is an extremely favourable environment for tropical cyclones to form. It was also concluded that some cases of tropical cyclones are found to form spontaneously from random convection; this due to the aggregation of convection as discussed by Bretherton *et al.* (2005).

Emanuel and Khairoutdinov (2010) explained how both a simplified model and a CRM can be used to simulate self-aggregation with different SSTs. From a review of previous studies, including some discussed here within this section, Emanuel and Khairoutdinov (2010) described conditions identified as necessary for self-aggregation to occur. These include;

small vertical wind shear of the horizontal wind, interaction of radiation with clouds and/or water vapour, and the effect of convectively enhanced surface winds on surface fluxes.

Emanuel and Khairoutdinov (2010) argued that the tropical atmosphere may have at least two stable equilibrium phases or states, built upon what was stated by Tompkins and Craig (1998a); one is convection that is random in time and space, and the second is the spontaneously aggregated convection. From these defined states and using the simplified and full model physics CRM, it was proposed that there is an abrupt phase transition between the two equilibrium states, which was dependant on the SST, with SST above a certain threshold allowing self-aggregation. The results from changing the SST values are displayed in figure 1.4, and there is quite a clear indication of a transition between the two phases of RCE, when the SST is near 297K. Above that threshold self-aggregation was observed to take place.

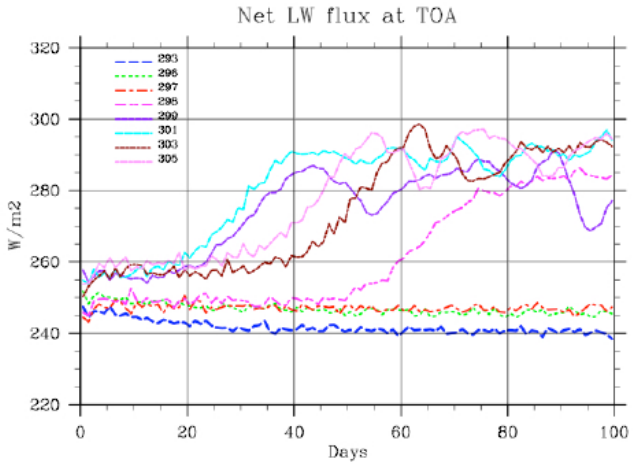

Figure 1.4 Net outgoing longwave flux averaged over top of the model domain, as a function of time, for eight values of the surface temperature using the CRM. (Source: Emanuel and Khairoutdinov, 2010, pp3)

Emanuel and Khairoutdinov (2010) tested a hypothesis derived from the statement, that there is a strong nonlinear dependence of self-aggregation on SST, 'that tropical convection can be in the state of a self-organized critically (SOC), which is analogous to the critical point in phase transition'. With an interactive SST, the model performed in accordance with the SOC hypothesis, reaching a state of SOC. From this investigation it was argued that the climate sensitivity of the SOC state is much lower (0.04 K/Wm^{-2}) than that of a uniform convection state (0.2 K/Wm^{-2}). Current climate models cannot simulate SOC states; therefore it could have an implication, as clouds provide high uncertainty levels within climate modelling.

1.4 Project Aims

As discussed in section 1.3 it has been demonstrated in a number of recent studies that to allow self-aggregation to occur there have been several conditions identified which are necessary for it to occur. These include; small vertical wind shear of the horizontal wind, interaction of radiation with clouds and/or water vapour, and the effect of convectively enhanced surface winds on surface fluxes.

The interaction between radiation and clouds/water vapour is deemed to be incredibly important as the radiation has positive feedback on the convection (Tomkins and Craig, 1998; Bretherton *et al.*, 2005; Stephens *et al.*, 2007). Destabilization by continuous large-scale radiation is one of the most important cloud-radiation interaction mechanisms (Tao *et al.* 1996).

It is known that convective clusters can maintain their structure and continue to grow when solar radiation is switched off. The modelling study investigated by Tao *et al.* (1996) stated that a topical squall line case did not show coherent cloud top cooling and cloud base warming. This was due to the presence of many clouds in this tropical oceanic squall line case that had varying cloud tops and bases. This result indicates that although cloud-radiation interaction seems to be essential for large-scale self-aggregation, it is not as important in producing smaller mesoscale structures like this squall line. The case study used by Tao *et al.* (1996) was a well-organized tropical oceanic squall system during the equatorial Mesoscale Experiment (EMEX).

The above review of these aggregation experiments therefore motivates us to investigate the radiation-cloud interaction relationship over the tropical ocean with fixed SSTs.

A key target of this study is to find out when the cloud-radiation interactions are actually taking an affect and driving self-aggregation to occur, as it is well known and documented that radiation interactions are needed for self-aggregation, and that it has a dominating effect on large scale structures. This will be contrasted with the radiative effects on the smaller scale structures in the first phase of equilibrium where convection is almost random in time and space, as described by Emanuel and Khairoutdinov (2010).

In the first part of the project the model results are compared with previous studies to check if self-aggregation is occurring and whether or not similar/suitable results are being produced by the model experiments described in section 2.1. We will also be looking at the effect that

the domain size and the convective parameterization scheme has on the aggregation occurring.

The model data is selected and analysed by the author through the use of the scientific programming language IDL, which is used to create visualizations out of the complex numerical data.

The second part of the report will investigate the relationship between radiation and the model domain. To do this three model runs will be compared, one with a fixed radiation heating profile, and two others both with interactive radiation schemes but on different grid lengths, 4km and 40km.

Chapter 2 outlines the model and model set-up. Methodology and results of the analyses through the model simulations will be presented in Chapter 3 and 4. Chapter 5 is a summary of the results presented within the study highlighting the limitations and areas of potential future work to be considered.

Chapter 2 – The model and experimental model set up

This section aims to briefly describe the main features of the Met Office Unified Model (MetUM) as set-up and used for the experiments in this project. The model runs were done as part of the Cascade program. This is a NERC funded consortium project to study organized convection in the tropical atmosphere using the Unified Model. The data was generated and supplied by Dr Grenville Lister and Dr Steve Woolnough, who are both working in the consortium project. From the model runs the author selected three model runs which are best suited to the needs of the project aims discussed in section 1.4. The three model runs selected are described in the following order in this chapter, experimental setup, and the key points selected from the parameterization schemes.

2.1 Experimental Setup

The basic model options and all experiments performed are summarized in Table 1. The model was run for three experiments from the cascade program with different schemes in place. Experiments NORAD and HIGHRES were run with 38 vertical levels and a horizontal grid spacing of 4km. The LOWRES experiment is also run with 38 vertical levels but has a horizontal grid spacing of 40km. The model solves non-hydrostatic, deep-atmosphere dynamics using a semi-implicit, semi-Lagrangian scheme as described by Davies *et al.* (2005). The initial conditions of all three experiments were set by a smaller domain spun up to reach radiative equilibrium, which are then used for the larger experiment domains.

TABLE 1. Summary of experiments

Experiment	Model domain	Grid Spacing (km)	Radiation Assumption	Subgrid Mixing	Runtime
NORAD	144 x 144 x 38	4	Fixed temperature increments	3d Smagorinsky	15 days
HIGHRES	144 x 144 x 38	4	Fully Interactive	3d Smagorinsky	60 days
LOWRES	200 x 100 x 38	40	Fully Interactive	BL sch. in vert.	30 days

For each experiment the interaction with external large scale processes and dynamics are to be ignored (as with many of the aggregation studies discussed in section 1.3), and therefore there is no imposed convergence into the domain, no forced uplift, no imposed wind shear and no Coriolis forcing. A fixed Sea Surface Temperature of 300K was used for the model, where it should be noted that Emanuel and Khairoutdinov (2010) suggest this is high enough

to get large-scale self-aggregation. The lateral boundary conditions are cyclic in both directions. The physics packages are discussed in more detail below.

2.2 Parameterization Schemes

This section introduces the METUM's comprehensive set of parameterization schemes used for the experiments set out in table 1.

2.2.1 Convection Scheme

The convection scheme of Gregory and Rowntree (1990) is used for all three experiments with a Convective Available Potential Energy (CAPE) closure. The Gregory and Rowntree (1990) scheme has a trigger dependant on the initial parcel buoyancy and a mass flux determined by a specified timescale for adjustment of CAPE.

The LOWRES 40km grid experiment uses a relative humidity dependant method for determining the adjustment timescale, which increases the amount of parameterized convection where the column is relatively moist.

The 4km grid experiments NORAD and HIGHRES uses a CAPE dependant convective parameterization which actually produces very little of the total rainfall. The Roberts (2003) modification of the Gregory and Rowntree (1990) scheme is used. This is set to have the same amount of convection as the default scheme in the limit of very low CAPE, but to have a very long CAPE-adjustment timescale at larger CAPE. The purpose of the modified scheme is to allow the parameterization to produce some shallow convection and some mixing. even However, the model at this grid spacing is able to resolve explicitly most of the deep convection and so the modification strongly damps down the parameterization in this limit. Unlike the LOWRES experiment there is no relative humidity dependence of the adjustment timescale in this scheme.

2.2.2 Microphysical scheme

The mixed phase cloud microphysics scheme is based upon Wilson and Ballard's (1999) scheme. It uses physically based transfer equations to predict ice as a prognostic variable. It uses the four water components of vapour, cloud liquid water, ice and rain to describe the moisture in the atmosphere. The transfer terms connect the four water components as in figure 2.1.

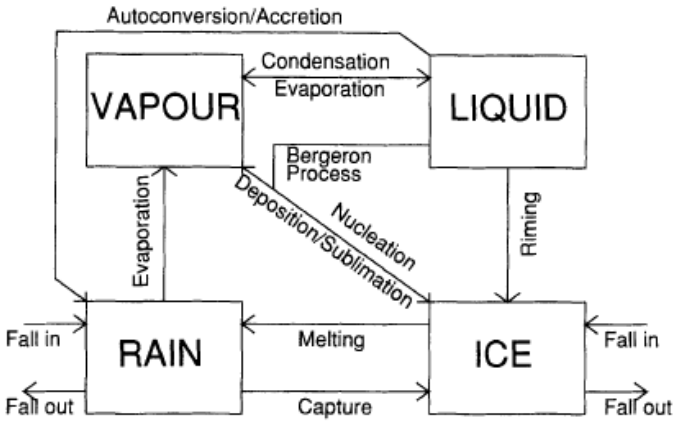

Figure 2.1 Schematic diagram showing the water quantities and the modelled transfers between them. (Source: Wilson and Ballard, 1999, pp 1610)

2.2.3 Radiation scheme

For all three model experiments there is no diurnal cycle included. Tompkins and Craig (1998a) stated that if the diurnal cycle were simply averaged over a day, a small zenith angle results, giving undesirable continuous long path lengths. Therefore the total amount of energy over a day is in fed in at a constant rate with a set solar zenith angle.

For the experiments HIGHRES and LOWRES the model has an integrated model radiation scheme based upon Edwards and Slingo (1996). This is a radiation code based upon the two-stream equations in both the long-wave and short-wave spectral regions. This means that processes that are important in both spectral regions, such as the overlapping of partially cloudy layers are treated time after time without fail. The two equations are only valid for monochromatic radiation, and hence the scheme performs a number of quasi-monochromatic calculations to solve the irradiance for a particular spectrum.

The code has a flexible spectral resolution enabling reference versions to be developed, that have high spectral resolution, which can also reproduce closely the results from line-by-line models.

As used in these experiments, the scheme calculates heating rates for both the long-wave and short-wave spectra at each model grid point. These calculations are based on the amounts of water vapour, CO2, ozone and all hydrometeor mixing ratios, with the effective radii of all water substances based on their mass mixing ratios.

The NORAD experiment employs a non-interactive radiation profile, which is fixed in space and time. For this experiment radiative heating/forcing profiles are derived from the domain

and time mean forcings from the 3d Smagorinsky HIGHRES model run for days 3 to 5 inclusive.

2.2.4 Boundary layer scheme

For the LOWRES 40km grid experiment, seven types of boundary layers are identified in the boundary layer parameterisation scheme: stable, stratocumulus over stable, well mixed, decoupled stratocumulus over cumulus, decoupled stratocumulus not over cumulus, cumulus capped and shear driven boundary layer. The first six of these are described by Lock *et al.* (2000) and the latest addition is the shear-driven type. The scheme described by Lock *et al.* (2000, pp3187) 'includes a representation of nonlocal mixing (driven by both surface fluxes and cloud-top processes) in unstable layers, either coupled to or decoupled from the surface, and an explicit entrainment parameterization.' It is important to note that other parameterizations within the model such as entrainment and convection are affected by the diagnosis of the boundary layer types.

For the HIGHRES and NORAD experiments turbulence is represented instead by a 3d Smagorinsky scheme based upon Smagorinsky's (1963) deformation-*K* closure scheme. There is no defined boundary layer scheme, other than this subgrid mixing turbulence representation.

Chapter 3 – Results Part (i) – Analysis of Self-aggregation

This chapter introduces the idea of self-aggregation by investigating; the relationship generated between precipitation and self-aggregation, the cloud structure and organization, and the equilibrium state.

3.1 Relationship between precipitation and self-aggregation

As discussed in section 1.3, the previous studies have shown that, during the approach to RCE, single clusters of aggregation form within the domain. This would indicate a trend from a large percentage of the domain experiencing precipitating events at the start of the run associated with random convection in space and time, and perhaps stratiform rain, to that number decreasing with time evolution.

Figure 3.1 is the domain is the domain daily averaged percentage of the domain with at least one precipitating event during the day of greater than 0.001mmday^{-1} for all three of the experiments. The HIGHRES and LOWRES experiments both with interactive radiation schemes indicate a decreasing trend in the percentage of precipitating events per day. The NORAD case has an increasing trend where the radiative forcing is fixed in space and time. Therefore from figure 3.1 we hypothesise that for large-scale self-aggregation to take place an interactive radiation scheme is needed. Within this chapter results are presented supporting this hypothesis.

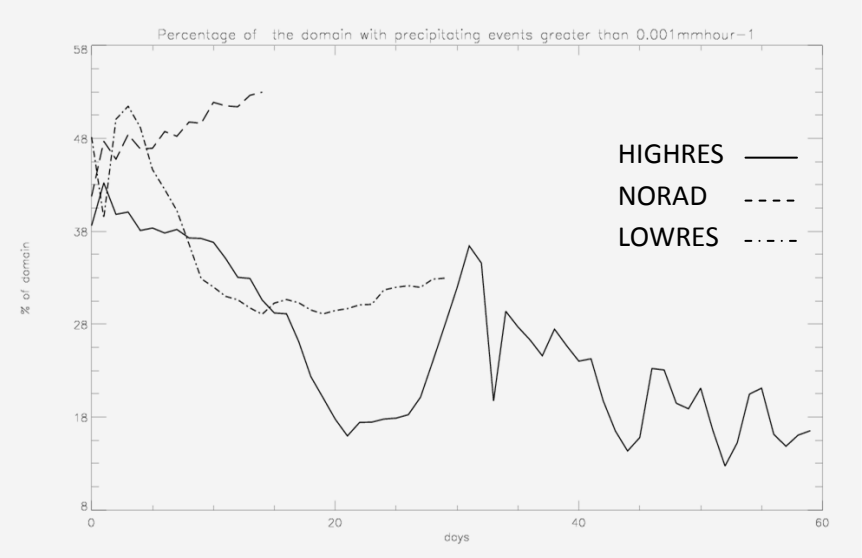

Figure 3.1 Domain and daily averaged percentage of the domain with at least one precipitating event during the day of greater than 0.001mmday^{-1}. For all three experiments.

3.2 Cloud Structure and organization

This section looks at the development and structure of the clouds in the time evolution to RCE, by the investigation into the following parameters; Outgoing Longwave Radiation (OLR) at the top of the atmosphere (TOA), and vertical cross-sections of cloud liquid water content (QCL), cloud frozen ice content (QCF), and vertical velocities.

a) Time evolution of OLR

Figures 3.2 and 3.3 are the daily time averaged plots for OLR at the TOA, for the HIGHRES and LOWRES experiments retrospectively. The NORAD experiment is not discussed here in terms of time evolution of OLR as this parameter is not available without a radiation scheme present. Figure 3.2 shows how the HIGHRES model is in a transient phase throughout the plots, and is best indicated by comparing day 1 (fig. 3.2(a)), where the convection is random in space and time, with day 60, where there is large-scale self aggregation observed (in blue). After day 10 the convection is observed to start to self-organize and perhaps move into phase of RCE, and this can be observed by the structures becoming organized in both shape and pattern. It is observed to form into bands (in blue), with a possibility of being squall line structures, of approximately 300km in length, which will also have high anvil cirrus associated with this, which as discussed in Chapter 1, has strong radiative properties. Alongside the aggregation the rest of the domain is observed to reach intense levels of OLR (in red), with values as high has 325 Wm^{-2}, indicating very dry regions, associated with strong radiative cooling of the atmosphere. The HIGHRES case is able to replicate the OLR structures observed in the previous idealized model studies discussed within section 1.4, bearing resemblance to Bretherton *et al.*'s (2005) figure (fig. 1.3).

Figure 3.3, is from the LOWRES experiment and data is available up to day 30. Initially on day 1, Fig. 3.3a, there seems to be randomly distributed convection, and perhaps some associated cirrus cloud within the domain. As it progresses, it starts to reach some sort of aggregated large scale state, backed up by fig. 3.0, and helping to prove the hypothesis. This is not as clear cut as for the HIGHRES experiment, as it is a considerably much larger domain, and has heavily parameterized convection based on relative humidity (RH). The scale of the aggregation clusters (in blue) are of the order of 400 to 500 km in horizontal width, which is larger than that observed in the HIGHRES experiment. This may be due to the fact that the domain size is larger and therefore clusters in HIGHRES cannot grow any larger. Domain size is not explicitly investigated any further. Around the cloud clusters, high

values of OLR (in red) are observed once again similar to that of the HIGH RES experiment indicating that there must be strong subsidence present.

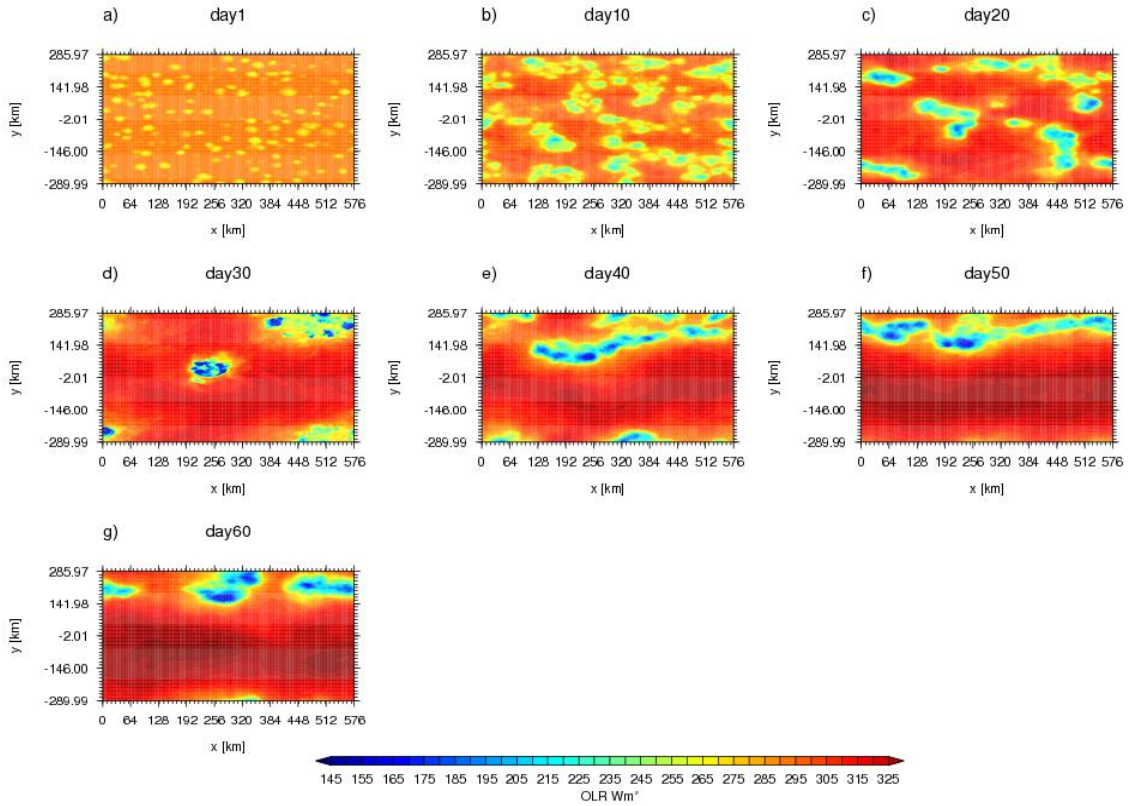

Figure 3.2 The HIGHRES experiment daily averaged OLR at the TOA, from days a) 1, b) 10, c) 20, d) 30, e) 40, f) 50, g) 60.

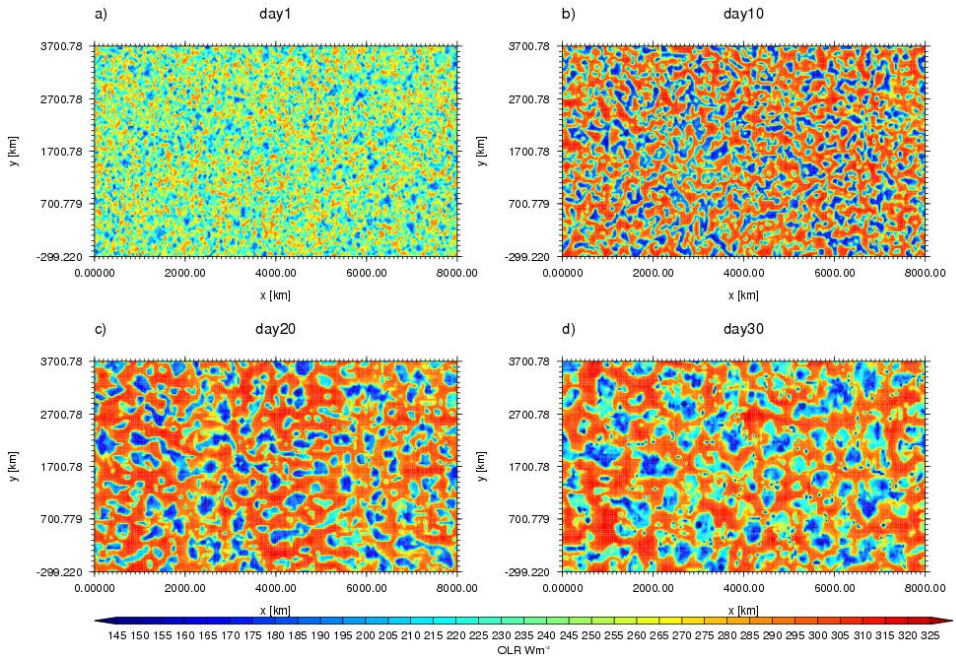

Figure 3.3 The daily averaged OLR at the TOA for the LOWRES experiment for days, a) 1, b) 10, c) 20, and d) 30.

b) Cloud structure at day 15

It is critically important to gain an understanding of why the NORAD experiment is not starting to self-aggregate as now observed in the HIGHRES experiment. To do this zoomed in 2D cross-sections have been taken at a time frame of, of QCL, QCF, and vertical velocity (w). It is appropriate to compare these two experiments as they are based on the same model schemes and the radiative forcing profile is the timed domain average from the HIGHRES model, as discussed in section 2.2.3. Figure 3.4(a) and (b) is a vertical cross section at Y=64.45km and Y=12.08km, for the HIGHRES experiment at 16:00:00 on days 15 and 59, and figure 3.5, for the NORAD experiment is a vertical cross section at Y=136.9km at 16:00:00 on day 15. The 2D cross-sections were selected from the targeted strongest vertical updrafts at z=5km.

Figure 3.4(a) indicates that the convection does not reach similar heights as that in the NORAD (Fig. 3.5) indicating it is still in the transient phase to RCE and across the domain, there a large number of strong associated convective updrafts. Here there are two cells picked up in this vertical y-section, with QCL values similar to that of the NORAD in Fig.3.5, of approximately 1.2gkg^{-1}. However the horizontal widths observed across the domain for the NORAD are of around 20km and the HIGHRES 5-10km.This gives an indication that both are still in a disorganized/random transient phase. By day 59 (Fig. 3.4b) the convection is penetrating higher into the troposphere, perhaps even to the tropopause, past the level of neutral buoyancy (LNB). The NORAD experiment has much higher levels of concentrated QCF, and also penetrates higher into the troposphere, with maximum values of 6.8gkg^{-1} compared to 3.5gkg^{-1} in the HIGHRES. Figure 3.5 shows that the NORAD has a strong convective core approaching a maximum of 10ms^{-1}, however the HIGHRES is only reaching a maximum of 7ms^{-1}. By day 59 (fig. 3.4a) there is a strong convective core approaching a maximum of 10ms^{-1} and higher associated QCF (6.8gkg^{-1}) values as opposed to those observed on day 15.

These values indicate that the NORAD experiment may have reached its peak disorganized phase, but it cannot be stated that it will not aggregate. But in the latter stages of deep convection (fig. 3.4b) that much of the QCL is swept out, which is not happening with the NORAD, Tompkins and Craig (1998a) also found this to occur in deep large-scale self-organized convection.

- FIGURE 3.4 -

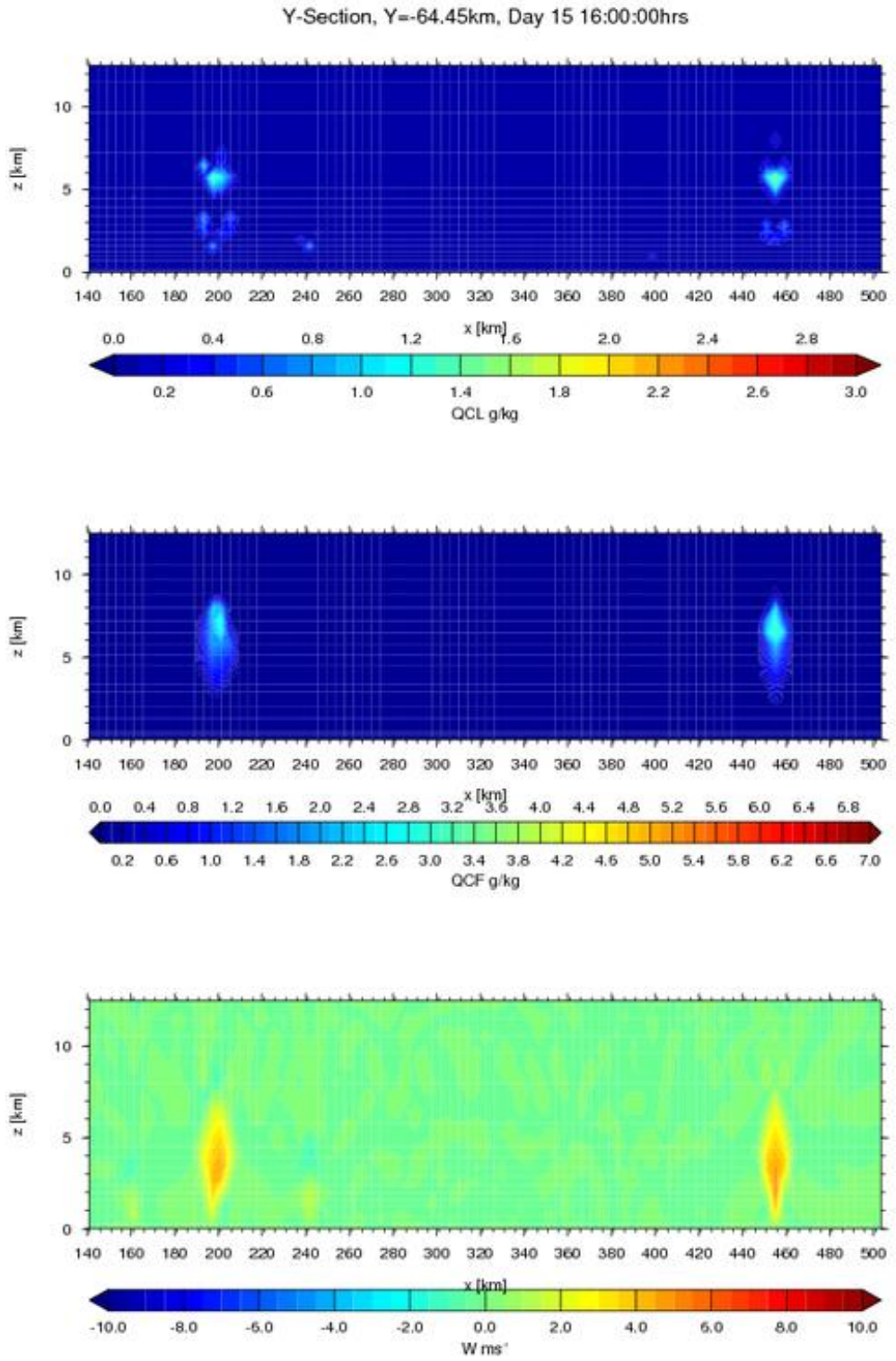

Figure 3.4(a) Time frames of QCL, QCF, and w for the HIGHRES experiment on day 15 at 16:00:00, at Y=64.45km.

- FIGURE 3.4 -

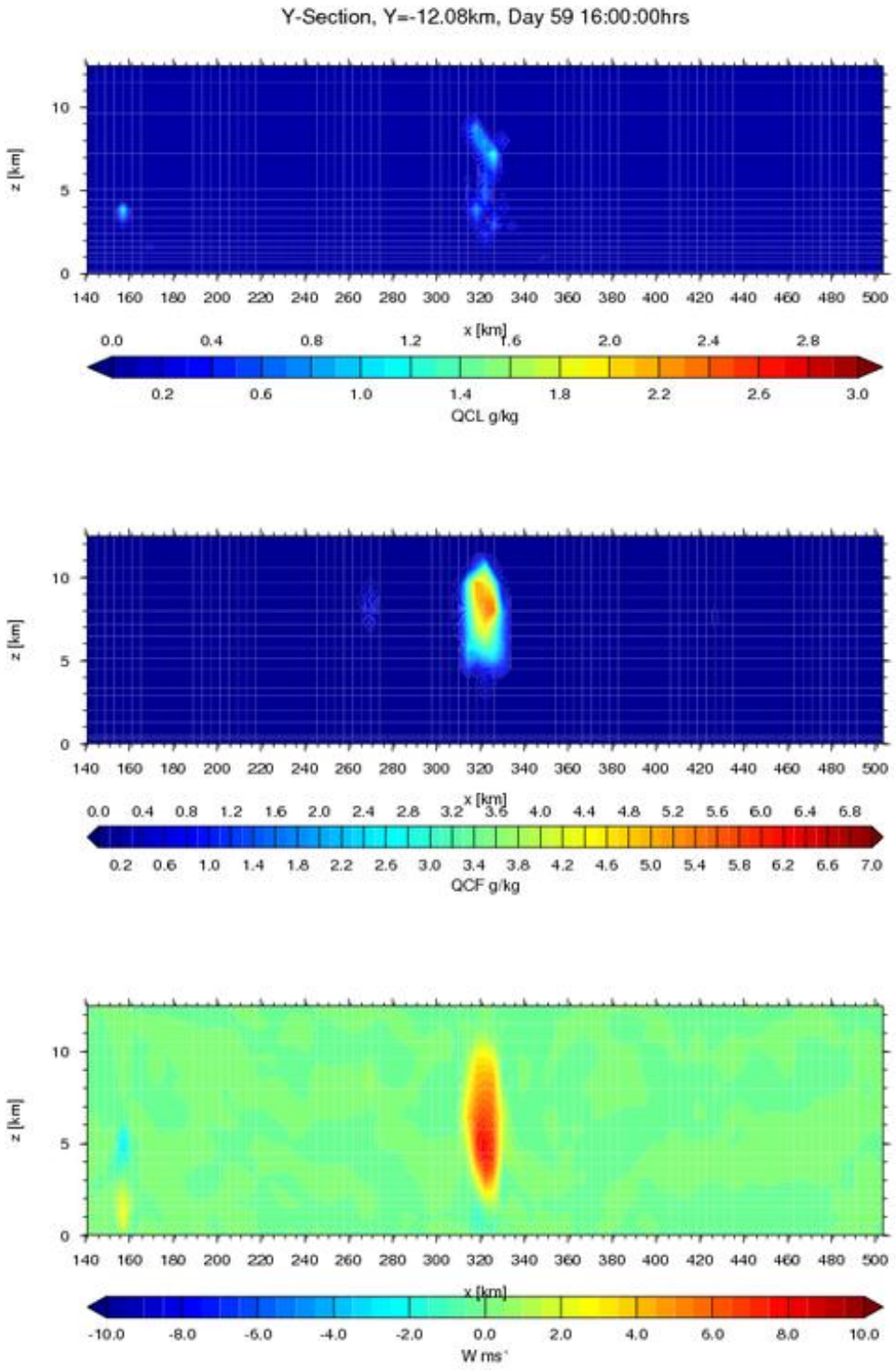

Figure 3.4(b) Time frames of QCL, QCF, and w for the HIGHRES experiment on day 59 at 16:00:00, at Y=12.08km.

- FIGURE 3.5 -

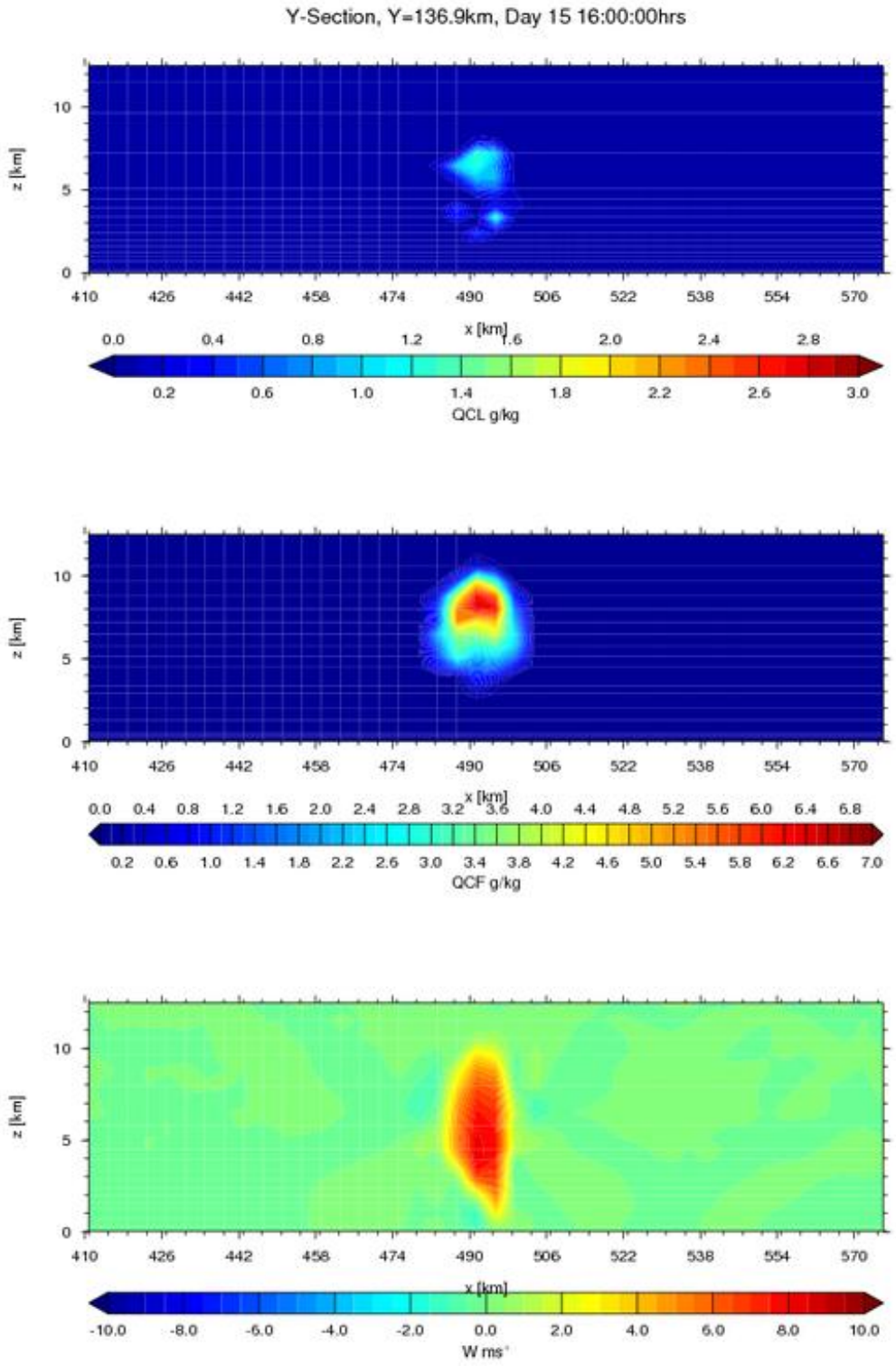

Figure 3.5 Time frames of QCL, QCF, and w for the NORAD experiment on day 15 at 16:00:00, at Y=64.45km.

3.3 Equilibrium State

As stated in section 1.2, to model the convection it is taken in its simplest form, Radiative Convective Equilibrium (RCE). This is where only radiation, convection and surface enthalpy are allowed to transfer energy in a 'two-way' transfer between each mechanism. Therefore it is important to understand when or if the model reaches the radiative equilibrium phase or state to test the hypothesis further. All three experiments listed in Table 1 are being investigated here to see if and when equilibrium is occurring.

a) (i) *QRAD and THF*

The approach to equilibrium can be understood from figure 3.6 which is a time series of the domain averaged net difference in Shortwave (SW) and Longwave (LW) radiation at the TOA minus the difference at the surface (QRAD) contrasted against the Total Heat Flux (THF) (latent heat flux plus sensible at surface), and the domain mean total precipitation. QRAD is defined in equation 1,

$$QRAD = ((SW_{TOA}\downarrow - SW_{TOA}\uparrow) - LW_{TOA}\uparrow)-(NETSW_{z(0)}\downarrow + NETLW_{z(0)}\downarrow) \quad (1)$$

where SW=shortwave radiative flux, LW=longwave radiative flux, and z(0)= surface level, the arrows represent whether the flux is acting downwards or upwards.

Figures 3.6(a) and (b) are for the HIGHRES experiment, Figs. 6(c) and (d) are the LOWRES results, and Figs. 6(e) and (f) NORAD experiment. The QRAD represents the total radiative cooling of the atmosphere, and therefore the difference between QRAD and THF at equilibrium would represent the role of the sea if it was able to interact. The difference will also have an impact on the Frozen Moist Static Energy (FMSE) introduced in section 3.3(b).

Figures 3.6(a) and 3.6(b) indicate that the HIGHRES experiment has a long time evolution of approximately 50 days (Fig. 3.6(a)), agreeing with Tompkins and Craig (1998b) that it typically takes 50 days for random convection to achieve RCE. The precipitation rate has a large fluctuation of total daily amounts from day 30 to 60, on 4 to 5 day timescales. Before day 30 it is on a shorter timescale but the fluctuations are not as large. Mesoscale convective cells are associated with much higher levels of precipitation rates.

Figures 3.6(c) and 3.6(d), alongside fig. 3.1, indicate that the LOWRES experiment is on its way to equilibrium, and may have reached it. From Fig. 3.6(d) it is clear to see that the daily precipitation rate does not have a similar short time-scale variability as the HIGHRES

experiment. However, it cannot be stated that it is not in Radiative Equilibrium, and this has been proven with figures 3.1 and figure 3.3 the daily mean OLR plots. The next few sections of this chapter will investigate the equilibrium state further with other parameters and techniques.

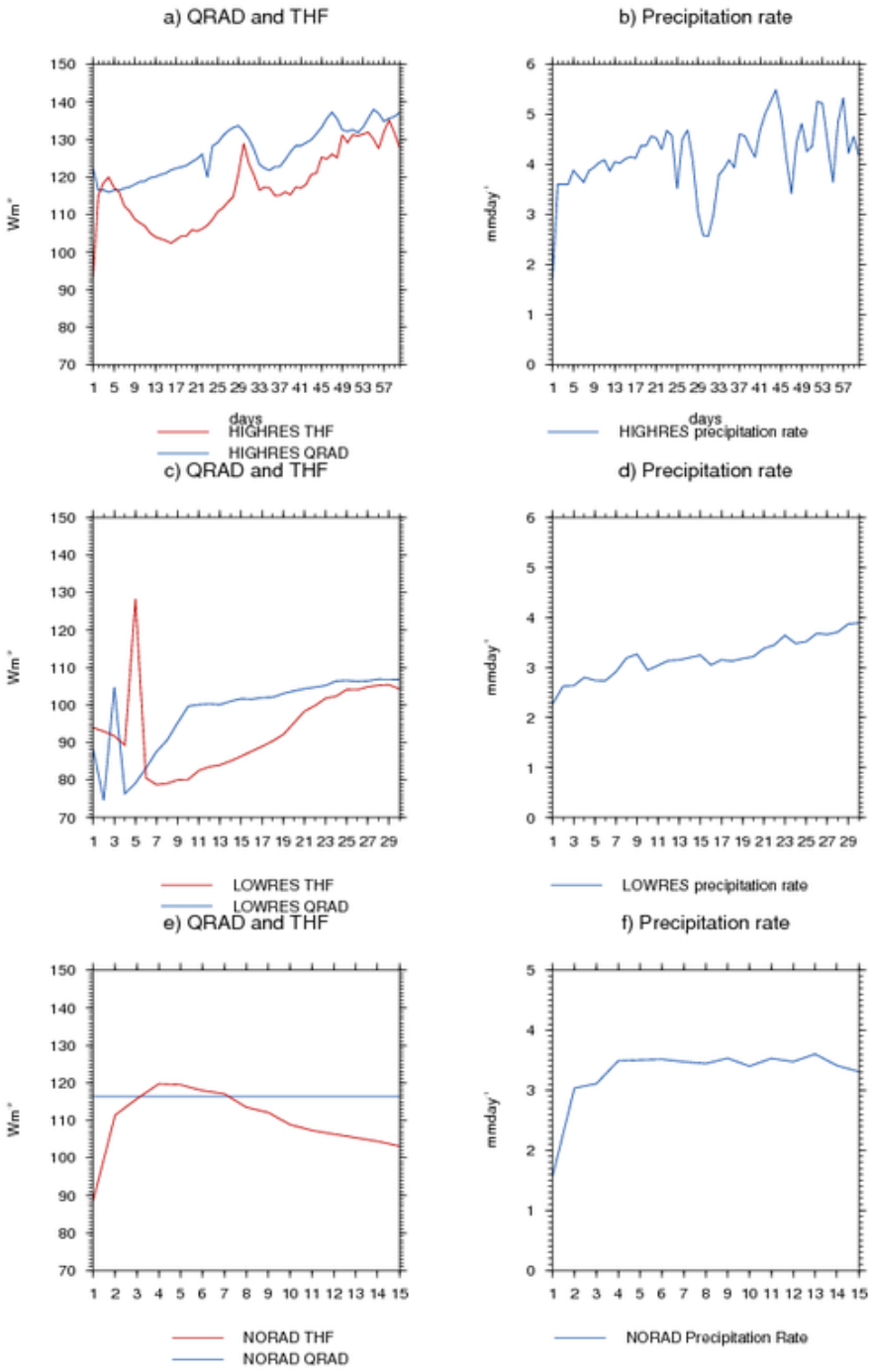

Figure 3.6 The time series of domain-mean averaged parameters QRAD , THF and precipitation rate, for a) and b) the HIGHRES experiment for 60 days, c) and d) LOWRES experiment for 30 days, and e) and f) the NORAD experiment.

Figures 3.6(e) and 3.6(f) indicate that the NORAD experiment may have reached equilibrium state, known as the first state as described by Emanuel and Khairoutdinov (2010). However without detailed research into this it is difficult to conclude that this is the case, future work has been suggested in section 5.3. When the domain is in an equilibrium state QRAD and THF are in balance as observed in the HIGHRES and LOWRES cases. In fig. 3.6(e) the THF is observed to decrease and as the difference between the two increases, FMSE is observed to increase (the implications of this are discussed in section 3.3(b)).

Fig. 3.6(f) shows the level of NORAD domain-mean daily precipitation rates levelling off, when compared against fig. 3.6(b) and 3.6(d), it is clear to see that it does not fit the trend of the other two experiments. The levels reached by the HIGHRES and LOWRES experiments are approximately 4.5mmday^{-1} and 4mmday^{-1} respectively, and indicate higher rates associated with deep large-scale self-aggregated convection observed in figures 3.2 and 3.3. These investigations so far have not shown if the NORAD experiment reaches a self-aggregated convection phase, whether or not it is small or large-scale organization, at 15 days runtime.

(ii) ***QRAD and THF*** **- HIGHRES -** ***Days 25 to 35 further analysis***

By day 30 there is a significant drop in the daily precipitation rate, which seems to coincide with the energy flux peaks observed prior to this day in fig. 3.6(a). Table 2 breaks down the significant values of the peaks and when they occurred.

From table two and fig. 3.6(a) and (b) we are able to see that there is definitely a relationship between the maxima observed in THF and QRAD on days 29 and 30 respectively, and the minimum precipitation value on day 31. It could be suggested that aggregation started to occur prior to this and then for some reason it has disorganized itself. There is also a delayed mechanism between the QRAD and THF maxima and the precipitation minima occurring. The peak in THF could either indicate a high flux of moisture into the atmosphere or perhaps a strong low-level cooling associated with regions of high OLR; this can be considered by looking at fig. 3.7. Figure 3.7 is the one day domain averages of OLR at the TOA for the HIGHRES experiment. With the approach to day 30 strong convective activity (dark blue, x=256km,y=-1km) is observed in fig. 3.7(d) where there are strong associated evaporation fluxes in the regions of convection, but also strong cooling due to the high regions of OLR (red) surrounding these cells. By day 31 (fig. 3.7e) it appears as if the strong convective cells have precipitated themselves out, hence the minima rainfall amount observed. Figure 3.1

shows that the percentage of precipitating events across the domain has increased from 18% at day 25 to 37% by day 30, maybe highlighting its return to the first stages of the transient phase in its evolution to an equilibrium state or perhaps some stratiform clouds left after the strong convection.

What is not clear is whether or not the sudden decrease in QRAD at days 23 could be the event for this trigger to occur, this is not investigated further here, however future investigations are highlighted in section 5.3.

TABLE 2. QRAD, THF and Precipitation rate comparison, HIGHRES experiment, Identifying the key values around day 30 from Fig. 3.6a.

Fields	Day 23	Day 25	Day 27	Day 29	Day 30	Day 31	Day 35
QRAD Wm^{-2}	120	130	132	134	132	130	122
THF Wm^{-2}	106	110	112	120	128	122	117
Precipitation $mmday^{-1}$	4.6	3.5	4.6	2.8	2.7	2.6	3.8

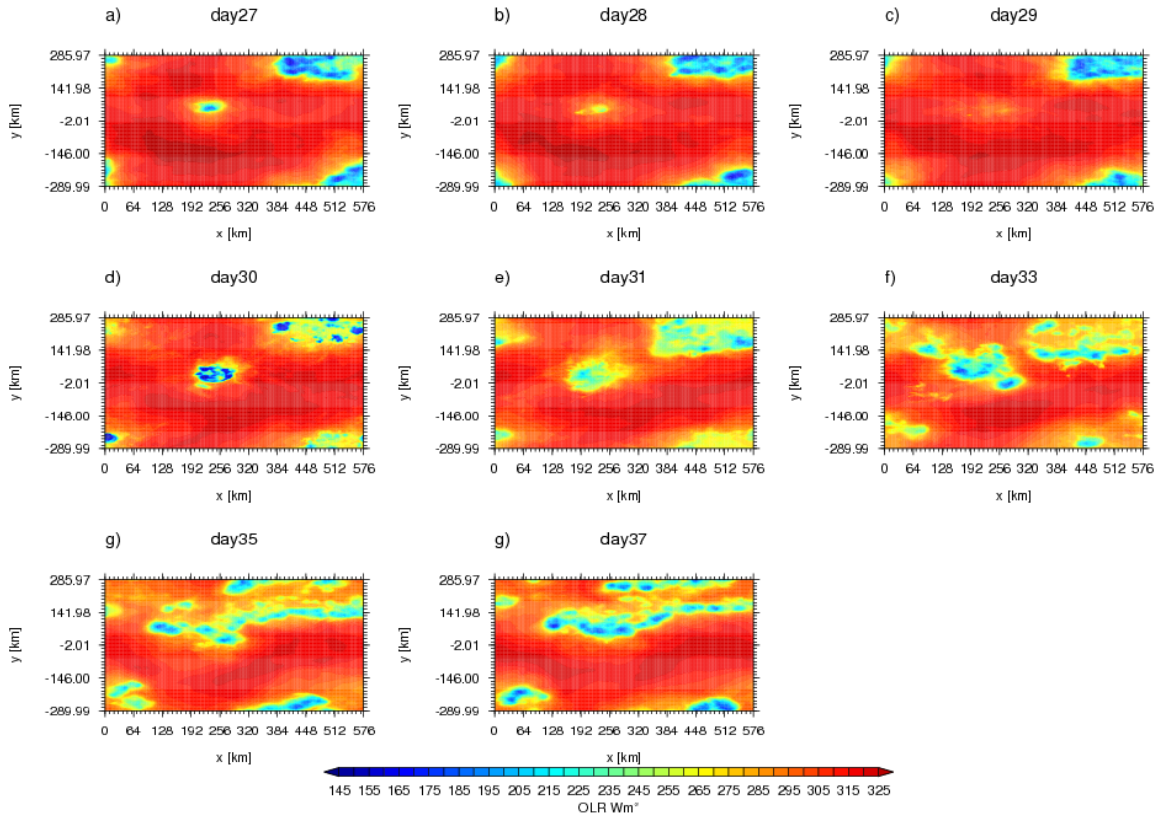

Figure 3.7 One day domain averages of OLR at the TOA for days, a) 27, b)28, c)29, d) 30, e) 31, f) 33, g) 35, and h) 37, for the HIGHRES experiment.

b) Frozen Moist Static Energy

The FMSE was defined by Bretherton *et al.* (2005), h_f as equation 2,

$$h_f = c_p T + gz + Lq_v - L_f q_{ice} \qquad (2)$$

where cp=1004Jkg^{-1}K^{-1}, the specific heat capacity for dry air, T is the temperature (K), g is the gravitational constant, z is the altitude, L_v=2.5x10^6 JKg^{-1} and L_f=2.826x10^6 Jkg^{-1} are the latent heats of condensation and of freezing, and q_v and q_{ice} are the mixing ratios of liquid water and ice. Moist static energy is a thermodynamic variable (analogous to equivalent potential temperature) which is calculated by lifting air parcels adiabatically to the TOA and allowing all water vapour to condense and release latent heat. It is a useful quantity for precipitating convection as it approximately conserved in adiabatic displacements of fluid parcels (Bretherton *et al.*, 2005).

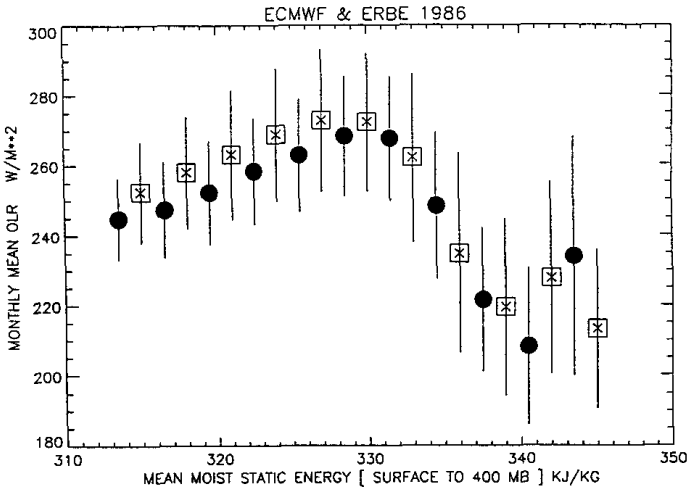

Figure 3.8 OLR as a function of moist static energy of the troposphere from the surface to 400mb in 1986. The OLR data were pooled into moist static energy bins from 315 to 345 kJkg^{-1} with a step of 3kJkg^{-1} before the mean and standard deviation were calculated. Circles represent oceanic grids and squares continental grids. (Source: Srinivasan and Smith, 1996)

Srinivasan and Smith's (1996) figure 3 (figure 3.8) indicates OLR as a function of moist static energy (MSE) of the troposphere (from surface to 400mb). The mean and standard deviation (s.d.) was calculated from data during the year of 1986. This data was pooled into moist static energy bins from 315 to 345kJkg^{-1} with a step of 3kJkg^{-1} prior to the mean and the s.d. being calculated. Figure 3.8 shows that from 313 to 330 kJkg^{-1} of MSE that OLR was observed to rise from 240 to 270Wm^{-2}. From 330 to 340kJkg^{-1} the observed OLR decreased to 200Wm^{-2}. For moist static energy greater than 340kJkg^{-1} the OLR is observed to increase

again. This is reversible as well. . The frozen part added to the equation as derived by Bretherton *et al.* (2005) was not subtracted from the moist static energy. Therefore a comparison has to be taken with careful consideration, as well as the fact that the calculations of h_f in this investigation include all levels of the atmosphere to include the maximum amount of ice content.

Figures 3.9(a), (c) and (g) represent the domain average of the time evolution of the vertical integral over pressure, of the time evolution of FMSE, for the HIGHRES, LOWRES, and NORAD respectively.

In comparison of fig. 3.9(a) and 3.6(a) of the HIGHRES experiment there is a clear link between h_f and the differences between QRAD and THF. From days 5 to 33 the general trend for QRAD and THF is to increase, but the difference between them becomes larger indicating an increase in h_f. As the difference between QRAD and h_f from days 33 to the end of the time evolution the h_f is observed to level off indicating the model has reached an equilibrium state. From days 1 to 33 with h_f increasing from 344.9 to 346.1kJkg^{-1} the mean OLR across the domain should rise in approximate comparison with fig. 3.8. This coincides with the total daily precipitation rate minima observed on day 31, as OLR is observed to increase across the domain in figure 3.7, with less dark blue convective cells present. The FMSE is then observed to lower and level off with a few fluctuations indicating self-aggregation and it fluctuations in size and strength from day-to-day.

In fig. 3.9(d) the LOWRES experiment the FMSE is observed to have an almost sinusoidal trend. The increase in hf corresponds well to the larger difference in QRAD and THF (fig. 3.6c), and then from day 21 an increase in h_f which may possibly lead to a levelling off after day 30, corresponds to the difference in QRAD and THF becoming significantly less. With this though we should experience higher values of OLR within the domain when compared to HIGHRES, and this is experienced in figure 3.3, where clusters seem to be forming and higher regions of OLR are observed between.

With the NORAD case h_f (fig. 3.9g) is observed to rise in level from 344.8 to 346kJkg^{-1} which matches the trend with the difference between QRAD and THF becoming larger (fig. 3.6e). When making an approximate comparison with figure 3.8 OLR should have an increasing trend, it can be speculated that either the domain is drying out due to aggregation starting to occur, or experiencing stratiform cloud types after convective events.

.c) Equivalent Potential Temperature and Vertical Velocities

The equivalent potential temperature (THETA_E) was calculated using equation 3, as,

$$\theta_e = T\left(\frac{P_o}{P}\right)^k \times RH^{(-r.R_v/c_p)} \times \exp\left[\frac{L_v.r_v}{c_p.T}\right] \qquad (3)$$

Where T is the temperature (K), L_v is the latent heat of evaporation for liquid water, c_p is the specific heat at constant pressure, as defined in section 3.1, b) retrospectively, r_v is the vapour mixing ratio, P_o=1000hPa is the reference pressure level, P is pressure level raised too, $k=(R_d/c_p)=0.286$, RH is the relative humidity, and $R_v=4.616x10^2$ $Jkg^{-1}K^{-1}$ is the gas constant for water vapour. This was calculated to produce THETA_E for all three experiments in Figs. 3.9b, e, and h.

Figure 3.9b is a time frame taken towards the end of the HIGHRES model run, when it has reached RCE, at the 80 metre model vertical level, a strong cold pool is located in a band across the middle of the domain at y=100km, with the low values in THETA_E associated with the high values of OLR at day 60 in figure 3.2(g). The LOWRES experiment features a higher proportion of the domain with higher values of THETA_E with few cold pools to balance this. The NORAD experiment by the end of the model run, has a large proportion of the domain associated with high values of THETA_E, with few cold pools.

Tompkins (2001b) argued in a study looking at the organization of tropical convection in low vertical wind shears, that the key to triggering new deep convective cells lies with the band of high THETA_E, but negatively buoyant air, situated inside the boundary of the spreading cold pools. Tompkins (2001b) states that it is this air that forms new convective cells. This could be further investigated to test the hypothesis further with the LOWRES and NORAD cases.

Another indication that the HIGHRES model has reached RCE is that there are a small number of isolated strong updrafts which are quasi-randomly distributed (Nolan *et al.*, 2007). The HIGHRES and LOWRES plots in figs. 3.9(c) and 3.9(i) indicate just this with updrafts of $7ms^{-1}$ at the 5km vertical level, which agrees with Nolan *et al.* (2007) figure 1. However the LOWRES experiment does not indicate any strong vertical updrafts, this is because this should be dealt with in the LOWRES by parameterization, and therefore this is not a clear diagnostic to test the hypothesis for this case.

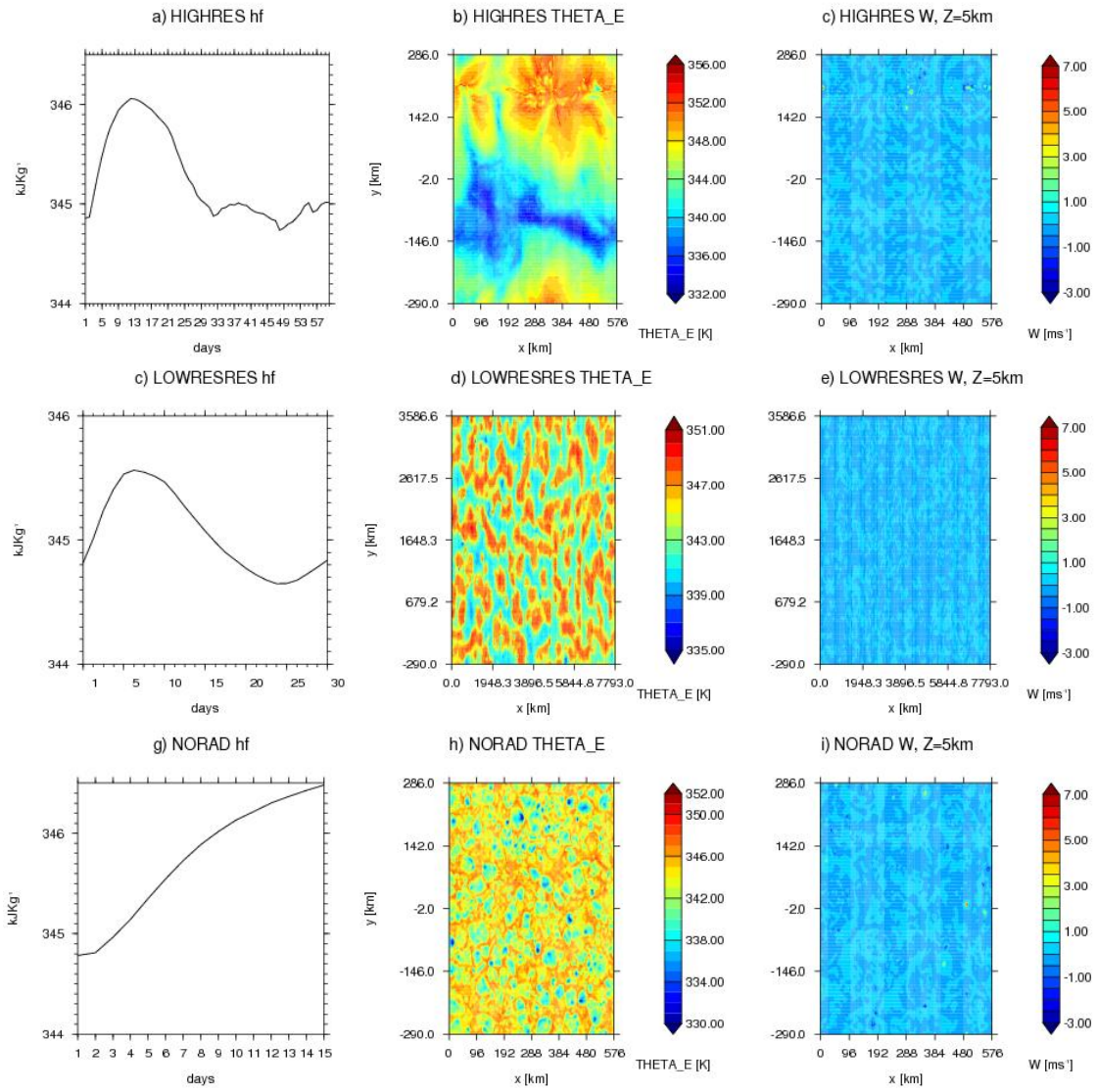

Figure 3.9 Illustration of the states of RCE in all three experiments as labelled: Time evolution of domain-averaged frozen moist static energy (kJ kg^{-1}) a), c), g), with timeframes in or near equilibrium for b), e), h) θ_e (K) on the vertical model level at 80m, and c), f), i) vertical velocity (ms^{-1}) at z=5km. All at 16:00:00 day 60, 30, 15.

d) Relative Humidity

Figure 3.10 shows the horizontally averaged profiles of Relative Humidity (RH) for all three experiments, with Fig. 3.10(a) for HIGHRES averaged on days 1 and 60, 10(b) LOWRES averaged on days 1 and 30, and 10(c) NORAD averaged on days 1 and 15.

Figure 3.10a shows that there is intense drying in the mid to upper troposphere outside the clusters of deep convection. This agrees well with the Bretherton *et al.* (2005) findings (Figure 4) whereby the day 50 average produced similar results.

Figure 3.10(b) sounding shows relatively little change in RH below 8km, with an actual increase in RH observed at 4.5km by day 30. This perhaps indicates an increase in cloud at this level across the domain, which may be a mixture of ice and water as the freezing level of 273.15K is approximately at 4.5km in height. However above the 8km height level drying is observed to be taking place, with perhaps an indication that LW radiative cooling is starting to take effect, and that aggregation of convective clusters is occurring on larger scales.

There is destabilization by radiation in the NORAD without the interactive radiation, it's just fixed in space and time, and does not respond to the current state its environment. In the NORAD case the RH is observed to increase below 8km in height by day 15. So this may indicate that for aggregation to occur a radiation feedback is needed, however Tompkins (2001a) was able to show without radiation feedbacks, small scale aggregation was observed. However Bretherton *et al.* (2005) found clusters to dissipate and removed aggregation after horizontally homogenizing the radiation. This will be investigated thoroughly in the next chapter.

In the HIGHRES and LOWRES cases (figures 3.10a and b) indicate more moisture at the upper levels of the troposphere, perhaps indicating a rise in the level of the tropopause or even moisture is penetrating into the stratosphere. Further work is suggested in section 5.3.

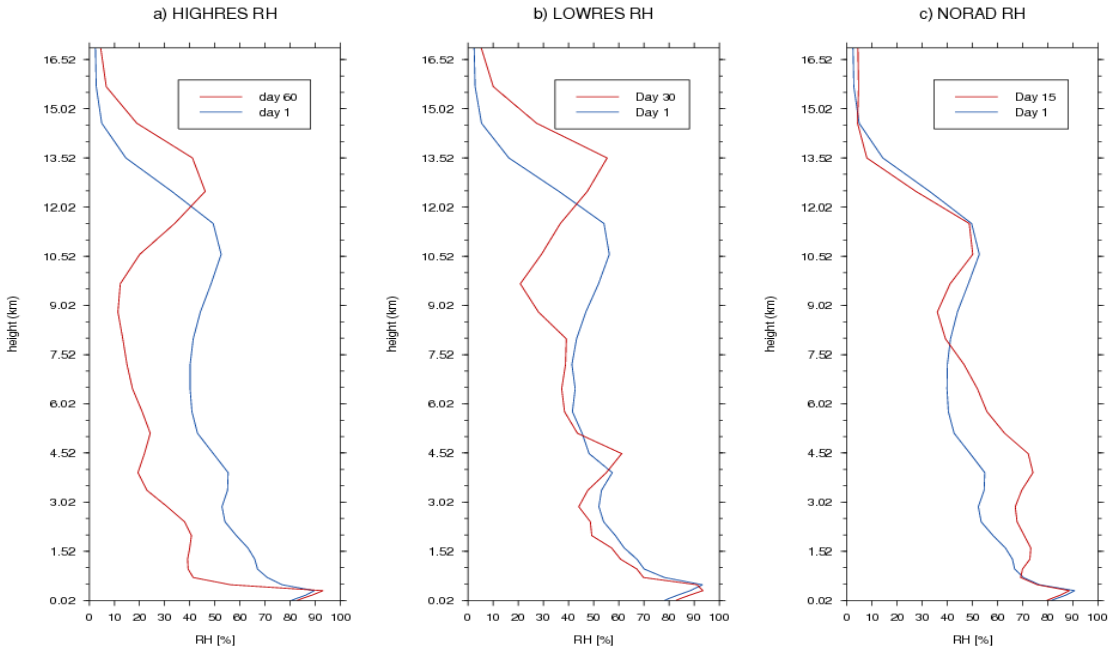

Figure 3.10 Horizontally averaged profiles of relative humidity for a) HIGHRES experiment averaged over days 1 and 50, b) LOWRES experiment averaged over days 1 and 30, and c) NORAD experiment averaged over days 1 and 15.

Chapter 4 – Results Part (ii) – Investigation into the radiation interaction effects, and fluxes generated

As previously stated in sections 1.3 and 1.4, it has been shown that an interactive radiation scheme is needed to allow interactive feedbacks between radiation, clouds and convection (e.g. Tomkins and Craig, 1998; Bretherton *et al.*, 2005; Nolan *et al.*, 2007; Stephens *et al.*,2009 ; Emanuel and Khairoutdinov, 2010). However as discussed in section 3.1(d), Tompkins (2001a) showed that small-scale convective aggregation can occur with a fixed horizontal radiation cooling, but Bretherton *et al.* (2005) found the opposite, that convection acted to disaggregate when horizontally-uniform radiation was imposed during the later stages of a model run.

Tao *et al.* (1996) claimed that from a model study that tropical squall lines did not show coherent cloud top cooling and cloud base warming. Within this chapter the author first investigates whether and when cloud top cooling and cloud base warming become coherent by looking at radiative heating profiles.

The second part of the investigation looks at the mechanisms involved which may trigger the aggregation, focusing on Bretherton *et al.*'s (2005) findings that as regions started to dry out, they started to radiatively cool more strongly in the lower troposphere than in the upper, and therefore bottom heavy radiative cooling had to be compensated by a bottom heavy subsidence profile. To drive this subsidence, a return flow from moist to dry regions in the lower to mid-troposphere developed above the boundary layer flow from dry to moist regions, and this circulation acted to amplify the self-aggregation.

4.1 Radiative Heating Profiles

a) Net Radiative Heating Profile

Figure 4.0 shows the vertical profiles of domain-averaged net radiative heating profiles, where the shortwave (SW) and Longwave (LW) profiles are subtracted from one another. Figure 4.0(a) is the HIGHRES experiment, averaged over days 55 to 60 inclusive, Fig. 4.0(b) is the LOWRES experiment, averaged over days 25 to 30 inclusive, and Fig. 4.0(c) is the NORAD experiment, for which the radiation is imposed as the averaged profile taken from the HIGHRES experiment for days 3 to 5 inclusive. The HIGHRES plot is when the domain is at approximately at RCE.

The net profiles observed in figure 4.0 shows how each model is able to replicate a typical tropical profile with a -1.5Kday^{-1} cooling rate. The LOWRES experiment in Fig. 4.0(b) shows strong net cooling between 8 and 9km in height. This maybe associated with the convection physics scheme which has parameterization of the cloud anvil effect. The area covered by convective cloud is needed as an input to the radiation scheme, and this is multiplied by a factor of three near the top of the cloud. Note that this factor is only applied to the convective cloud from the convection parameterization itself, and therefore any "large-scale" cloud (which forms above a certain relative humidity level) which is not affected by the scaling function. The HIGHRES and NORAD experiments do not show such strong net radiative cooling within the upper troposphere. However all three experiments show clearly that there is strong net radiative cooling either associated with the boundary layer or just above it. The impact of this will be discussed in section 4.1(b).

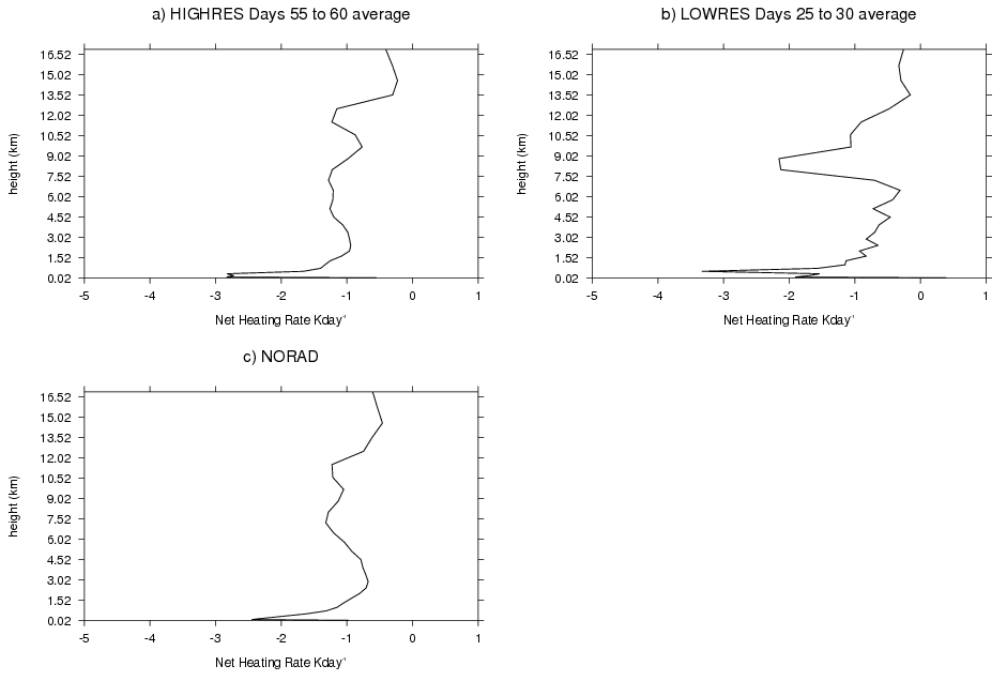

Figure 4.0 Vertical profiles of domain-mean net radiative heating, a) HIGHRES experiment, averaged over days 55 to 60 inclusive, b) LOWRES experiment, averaged over days 25 to 30 inclusive, c) NORAD experiment, the HIGHRES averaged profile for days 3 to 5 inclusive.

Due to long wave cooling above the clouds you would expect all three profiles to reach the level of zero net radiative heating. Figure 4.0 shows that there is considerable net cooling up to 10km and more in all three experiment. However at 15km in height for the NORAD and HIGHRES, and at 13.5km for the LOWRES experiments, the profiles do approach zero. Previous sensitivity studies have indicated that if clouds are present, they should act to raise

the level of net zero heating (Mather *et al.*, 2007). The associated decrease in cooling above these observed levels is caused by a combination of the drop-off in radiative cooling as the concentration of water vapour decreases with temperature, and also heating in the ozone and carbon dioxide bands.

b) Radiative Heating Profiles, Precipitating/Non-Precipitating

Heating rate profiles indicate and provide the links between cloud properties, large-scale dynamics, and radiation (Mather *et al.*, 2007). The domain-average radiative heating rates have been separated into two categories, precipitating (areas $\geq 0.001 mmhr^{-1}$), and dry (areas < $0.001 mmhr^{-1}$) (where it is the total amount of rainfall over a day and the precipitation points are those when the average rain rate is at least this number) to investigate the links highlighted by heating rate profiles. From figure 3.1 it has already been hypothesised and proven in chapter 3, that aggregation is occurring with the interactive radiation schemes, as the HIGHRES and LOWRES experiments show a decreasing trend in the percentage of the domain with precipitating events as opposed to the NORAD experiment in which this fraction is increasing. As the NORAD has fixed radiative forcing dictated by the day 3 to 5 horizontally averaged heating rate from HIGHRES, the author is using figures 4.1 and 4.2, to investigate the radiative heating for HIGHRES and LOWRES respectively.

Figures 4.1 and 4.2, (i)(a), (ii)(a), (iii)(a), and (iv)(a) are the daily domain-averaged LW and SW heating profiles split between precipitating and dry regions. Figures 4.1 and 4.2 (i)(b), (ii))(b), (iii)(b), and (iv)(b), are the daily domain-averaged net radiative profiles for the precipitating regions, dry regions, and the whole domain. Both figures include days 15, 20, and 25, but fig. 4.1 also includes the mean value taken for days 55 to 60 (fig. 4.1(iv)) when the HIGHRES experiment has reached equilibrium. Only the LOWRES and HIGHRES heating profiles are investigated within this section due to the fact that the NONRAD case is fixed in space and time.

Firstly it is useful to gain an idea of timing for when the radiation heating profile is changing due to aggregation and this can be understood from the net radiative heating profiles for both the LOWRES and HIGHRES experiments in figs. 4.1 and 4.2. The profiles between the dry and precipitating regions separate, in both experiments and it can be depicted that when the precipitating points decrease in number, an increasing percentage of the domain becomes drier due to aggregation. An indication of this aggregation occurring is that there is less domain-averaged radiative cooling in the precipitating (cloudy) regions. This is due to the

localized radiative effects of high clouds in the precipitating regions that heat the upper troposphere mostly at the bases of high thick cloud with associated cooling from the top, and Stephens *et al.* (2008) claim that this is the basic source of the moist-dry radiative heating gradients. The dry net profiles in the HIGHRES and LOWRES (fig. 4.1 and 4.2) are similar throughout each case study, but quite different to each other. This is because these are determined by the moisture profiles and the clear-sky temperature (Stephens *et al.*, 2008).

In the HIGHRES experiment within the precipitating regions, the effect the weaker radiative cooling occurs over a section of the troposphere between 3 to 9km at day 15 (fig. 4.1(i)) and this extends further to a height of 11km by day 25 (fig. 4.1(ii)). In the LOWRES experiment, there are larger differences between the dry and precipitating regions. There is a net warming with a maximum observed of 1.5Kday^{-1} as opposed to a decrease in net cooling to -0.8Kday^{-1} in HIGHRES, at day 15 (fig. 4.2(i)). This region of net radiative warming is within a section of the tropopause between 3 to 9km although the top of this region decreases in height to 7.5km by day 25 (fig. 4.2(iii)).

At 12km in the HIGHRES experiment (fig. 4.1(i),(ii),(iii)) the net radiative heating in the precipitating regions displays an increase in the net cooling through the transient period of the plots, perhaps associated with anvil cirrus diverging from the aggregating regions. This has a net warming effect on the troposphere below as just discussed previously. The opposite is the case for the LOWRES experiment (fig. 4.2(i),(ii),(iii)), in which the net cooling is observed to break into two distinct segments of perhaps cirrus cloud in the upper troposphere by day 25. The first is at a height of 7 to 9km associated with a deep gradient and perhaps indicating high optical thickness (Mather *et al.*, 2007), and the second is at 9 to 13.5km in height, of perhaps low optical thickness but greater depth, which may indicate why there is a drop in height of the observed warming in the precipitating regions.

There are notable differences in the net radiative profiles between the dry and wet regions in both HIGHRES and LOWRES. In the HIGHRES experiments the largest differences are observed by day 20 (Fig. 4.1(ii)), and in the case of the LOWRES experiment (Fig. 4.2(ii)) also by day 20 with the separation of upper level dry heating rates into two separate bands. The separation occurs with a decrease in net cooling, and this may coincide with the RH profile in figure 3.10(b) where the profile is observed to dry in the upper troposphere by day 30. However above this dry level at 12km in fig. 3.10(b) the RH increases, perhaps indicating that moisture transport is tending to push the tropopause level up with very deep strong

convection passing the Level of Neutral Buoyancy (LNB), or penetrating into the stratosphere. Figure 4.2 suggests that the tropopause level is at 13.5km for the LOWRES experiment, and therefore this increase in RH could indicate that convection is trying to raise this level. Figure 4.1(i),(ii),(iii) indicates that for the HIGHRES experiment the tropopause is holding at a level of 13.5km.

Secondly we investigated when cloud top cooling and cloud base warming becomes apparent. It is known that heating in the lower sector of the cloud is due to the temperature difference between cloud base and the surface below. The opposite is true for the cloud top. To produce cloud top cooling, clouds must be optically thick, otherwise LW heating is observed.

The shortwave profiles show heating in the upper troposphere in both the HIGHRES (fig. 4.1(i),(ii),(iii)) and LOWRES experiments (fig. 4.2(i),(ii),(iii)) within the dry and precipitating regions, due to absorption by water vapour and ice within the troposphere. All of the profiles in both experiments show SW cooling due to clouds in the precipitating regions throughout the lower troposphere, with peak cooling occurring below the base of the low cloud layer within the boundary layer in the dry regions.

There is a sharp heating gradient in the SW and LW profiles across a layer between 9 and 12km (HIGHRES) and 7 and 9km (LOWRES) by day 25, indicating that the layer of cloud may well be optically thick, caused by the presence of a high concentration of ice hydrometeors. Below this region in both the LOWRES and HIGHRES there is an increase in LW radiative heating, due to the ice clouds, and the peak is notably lower in altitude than the SW heating peak and is approximately at the base of the cirrus region in the precipitating areas.

- FIGURE 4.1 -

Vertical profiles of domain-average radiative heating for the HIGHRES experiment, where for each day, the heating rate has been averaged for precipitating areas $\geq 0.001 mmhr^{-1}$, and for dry regions $<0.001\ mmhr^{-1}$

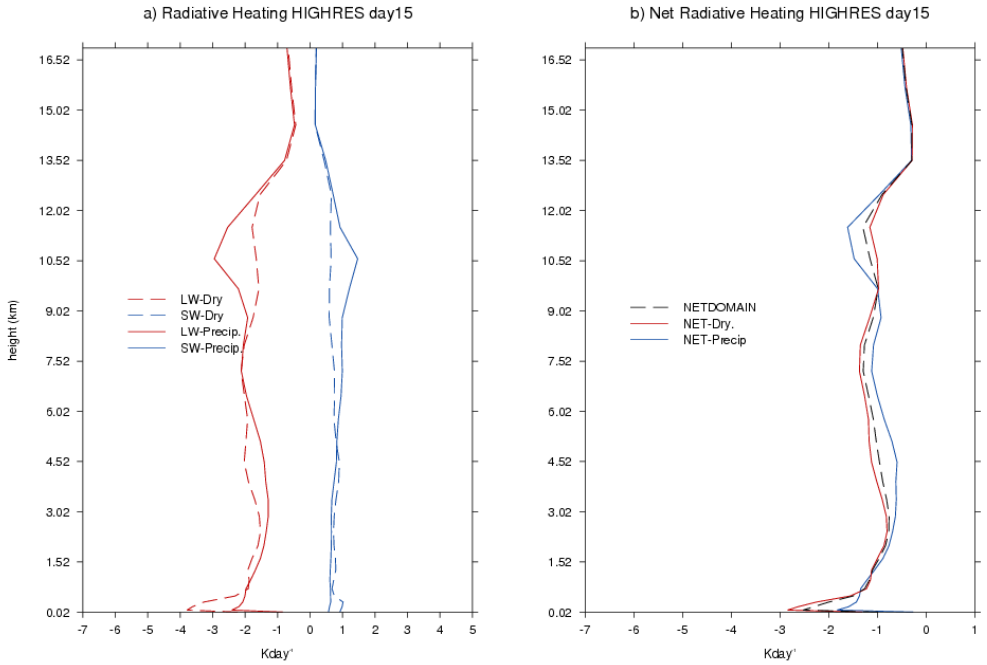

Figure 4.1(i) radiative heating LW and SW profiles (a) and the net radiative heating (b) for the HIGHRES experiment for day 15.

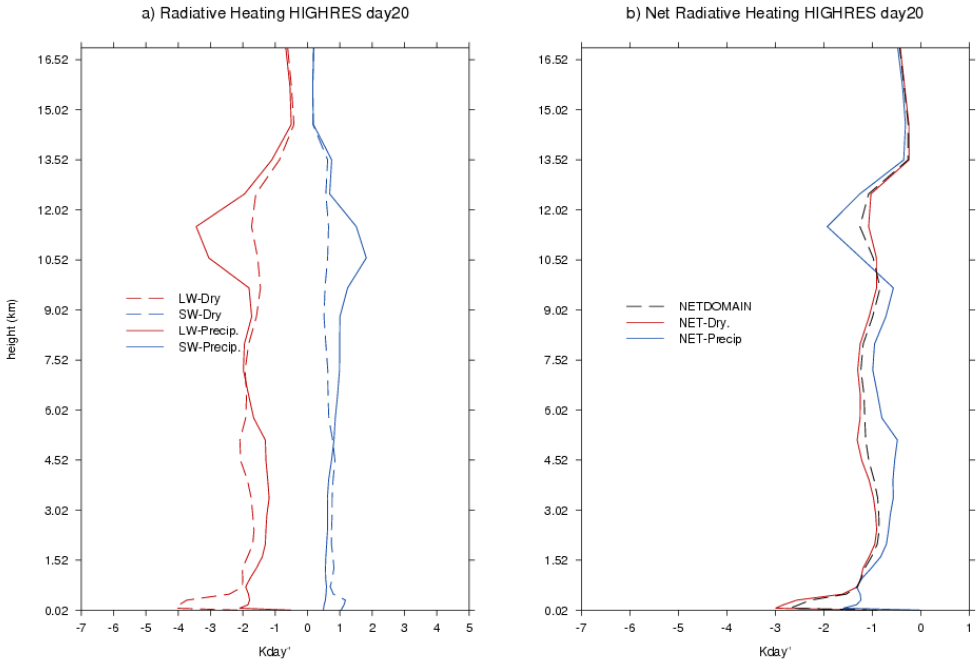

Figure 4.1(ii) radiative heating LW and SW profiles (a) and the net radiative heating (b) for the HIGHRES experiment for day 20

- FIGURE 4.1 -

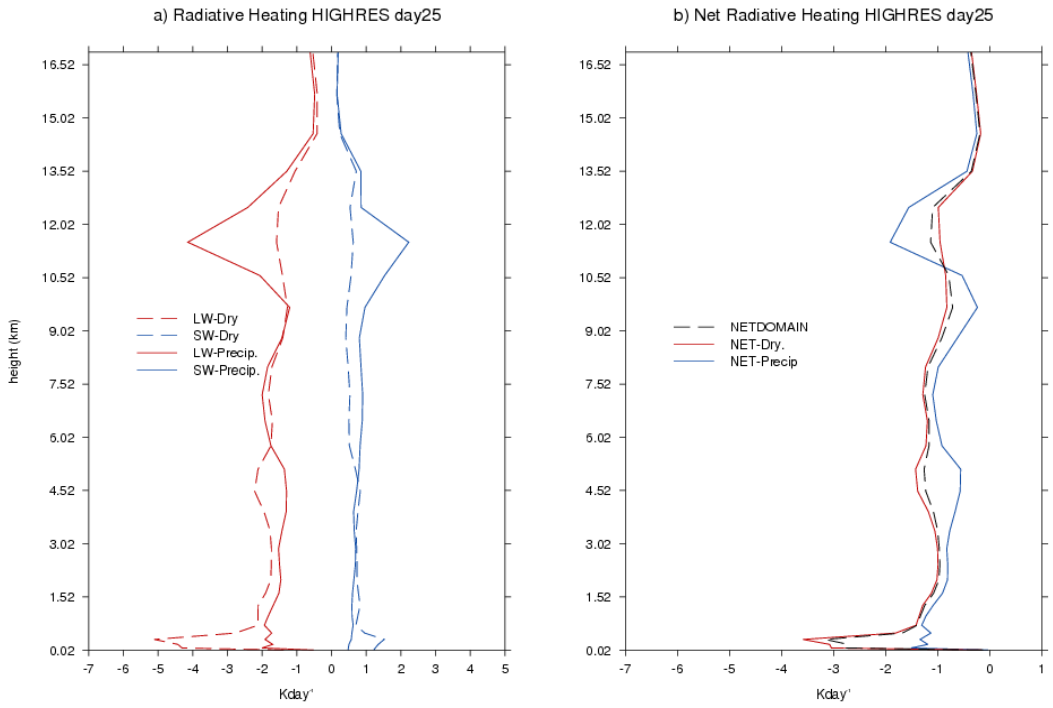

Figure 4.1(iii) radiative heating LW and SW profiles (a) and the net radiative heating (b) for the HIGHRES for day 25.

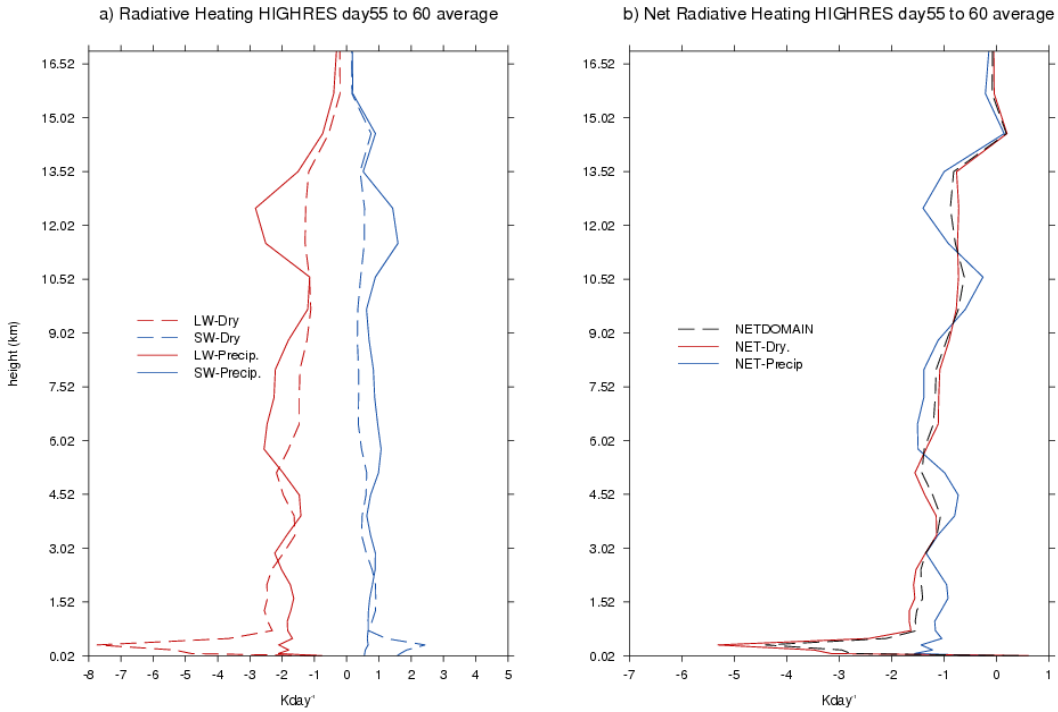

Figure 4.1(iv) Radiative heating LW and SW profiles (a) and the net radiative heating (b) HIGHRES for days 55 to 60 inclusive domain average.

- FIGURE 4.2 -
Same as figure 4.1, for the LOWRES experiment for days 15, 20, and 25.

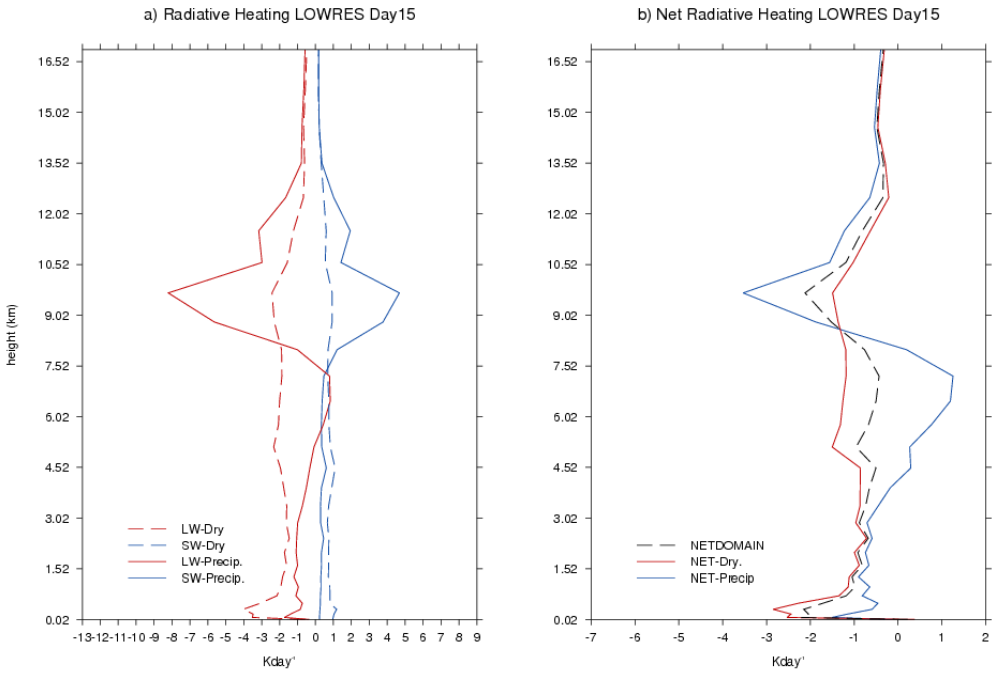

Figure 4.2(i) radiative heating LW and SW profiles in plot a) and the net radiative heating in plot b) for the separated into dry and precipitating regions for LOWRES for day 15.

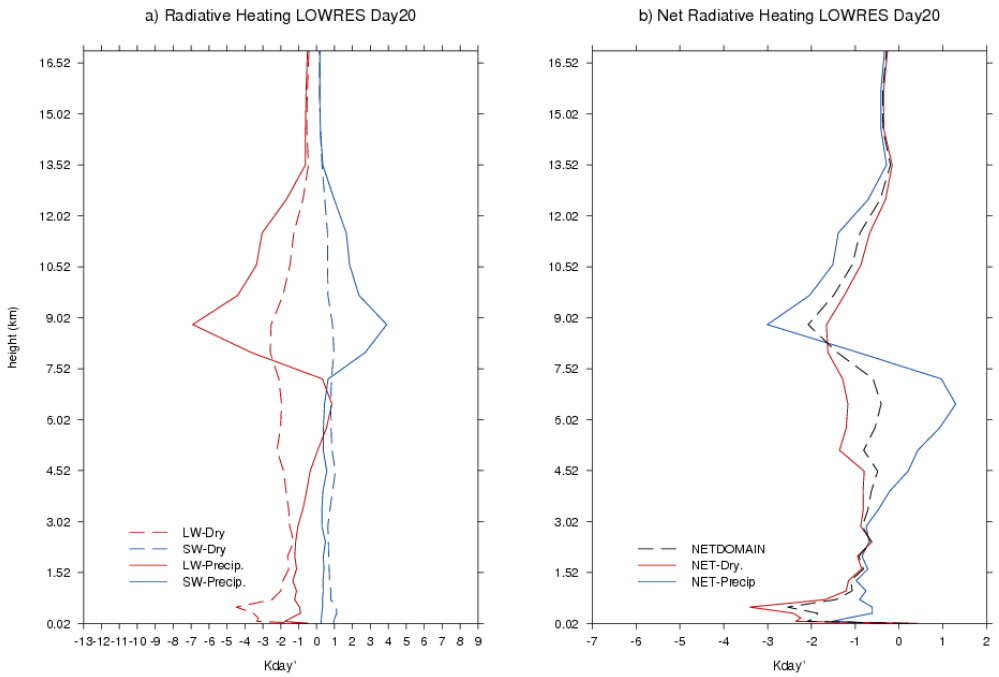

Figure 4.2(ii) radiative heating LW and SW profiles in plot a) and the net radiative heating in plot b) for the separated into dry and precipitating regions for LOWRES for day 15.

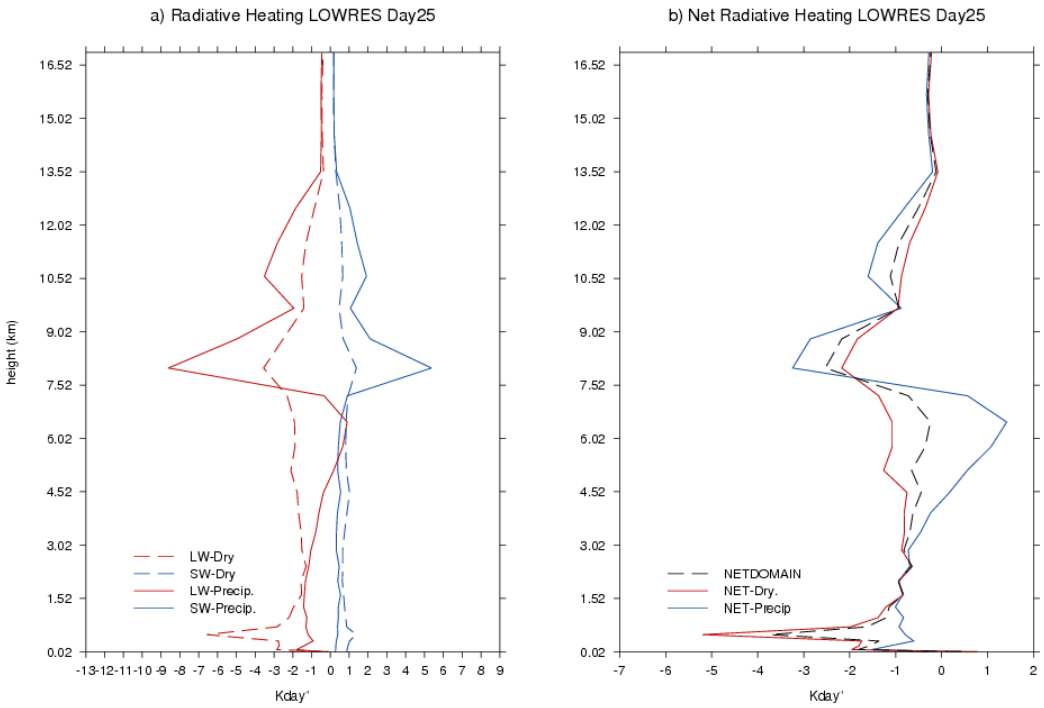

Figure 4.2(iii) radiative heating LW and SW profiles in plot a) and the net radiative heating in plot b) for the separated into dry and precipitating regions for LOWRES for day 15.

The peak in SW heating corresponds to the height at which the peak in ice cloud occurs (further discussed in the next section 4.1(c)), while the LW cooling peaks towards the top of the cloud. The amount of high cloud in the LOWRES experiment is providing much larger amounts of LW cooling in the precipitating regions.

The HIGHRES plots indicate that there is a clear and coherent structure of different levels of clouds within the precipitating regions indicated. However, the coherency of cloud top cooling and cloud base warming does not become particularly clear until day 20 when aggregation is observed to occur in the OLR plots in figure 3.2(c). This is because there is a higher proportion of ice clouds in the upper troposphere and liquid water clouds in the lower troposphere. In the LOWRES the cloud base warming and cloud top cooling is quite obvious and this may be due to the cloud anvil parameterization discussed in section 4.1(a) from day 10 onwards. The RH is also observed to drop in the upper troposphere (figure 3.10b), and therefore by day 25 less large-scale cloud will form at this level as the RH is used to determine whether such cloud occurs. So the cloud top cooling level is expected of to drop in vertical height.

There is a pronounced LW difference between the dry and precipitating regions, which could be associated with boundary layer clouds, whereby there is cooling within the cloud layer and heating below the layer. There may also be significant SW heating associated with the cloud layer. To investigate the LW cooling in the boundary layer for the LOWRES experiments the boundary layer type diagnostics were investigated. These diagnostics are produced by the boundary layer parameterization used and were not available for the HIGHRES experiment as turbulence is represented by 3d Smagorinsky as discussed section 2.2.4. Table 3 represents the percentage of the domain that has a given boundary layer diagnostic, averaged over, days 1 to 25 inclusive, for the LOWRES experiment. This indicates that 50.89% of the boundary layer has some form of convective cloud capping it, whether it be cumulus or stratocumulus. This could indicate why there is such strong LW cooling in the dry and precipitating regions; however the next section 4.1(c) will investigate further by using the cloud liquid water and ice contents diagnostics within the dry and precipitating regions. What is interesting to see is that approximately half of the domain is wind shear driven, and therefore one would expect high Latent fluxes associated with this. The strong LW cooling at the boundary layer in the dry regions may just be due to the large scale drying of the non-cloudy regions.

TABLE 3. Boundary Layer Diagnostics for the LOWRES experiment from day 1 to 25

Diagnostic	Percentage of Total Domain
Stable BL	0%
Stratocumulus over stable BL	0%
Well-mixed BL	3.26%
Decoupled Stratocumulus not over Cumulus	3.08%
Decoupled Stratocumulus over Cumulus	0.65%
Cumulus Capped BL	43.9%
Wind Shear Driven	49.11%

Figure 4.3 is the domain-averaged vertical profiles of specific humidity (q), for (a) HIGHRES, averaged over days 15 to 25, (b) LOWRES, averaged over days 15 to 25, and (c) NORAD, averaged over days 5 to 15. In the HIGHRES experiment the boundary layer has very high levels of q, and above this layer the free troposphere is dropping significantly with a sharp gradient (almost vertical) between the two observed at 1km in the dry region. This is happening in the LOWRES case too, but the sharp gradient in q is observed at 3km in height.

There is a clear difference in q between the dry and precipitating regions in both the HIGHRES and LOWRES experiments. With less q in the dry regions, less radiation is absorbed and emitted by water vapour, hence the strong LW cooling observed in the HIGHRES and LOWRES cases. There are no observed large differences in q for NORAD due to the fact that the radiation is not allowed to change to the environment, which affectively controls by the convective feedbacks. All three experiments present high values of q, and Tompkins and Craig (1998a) found that bands of organized convection are associated with high boundary layer moisture levels.

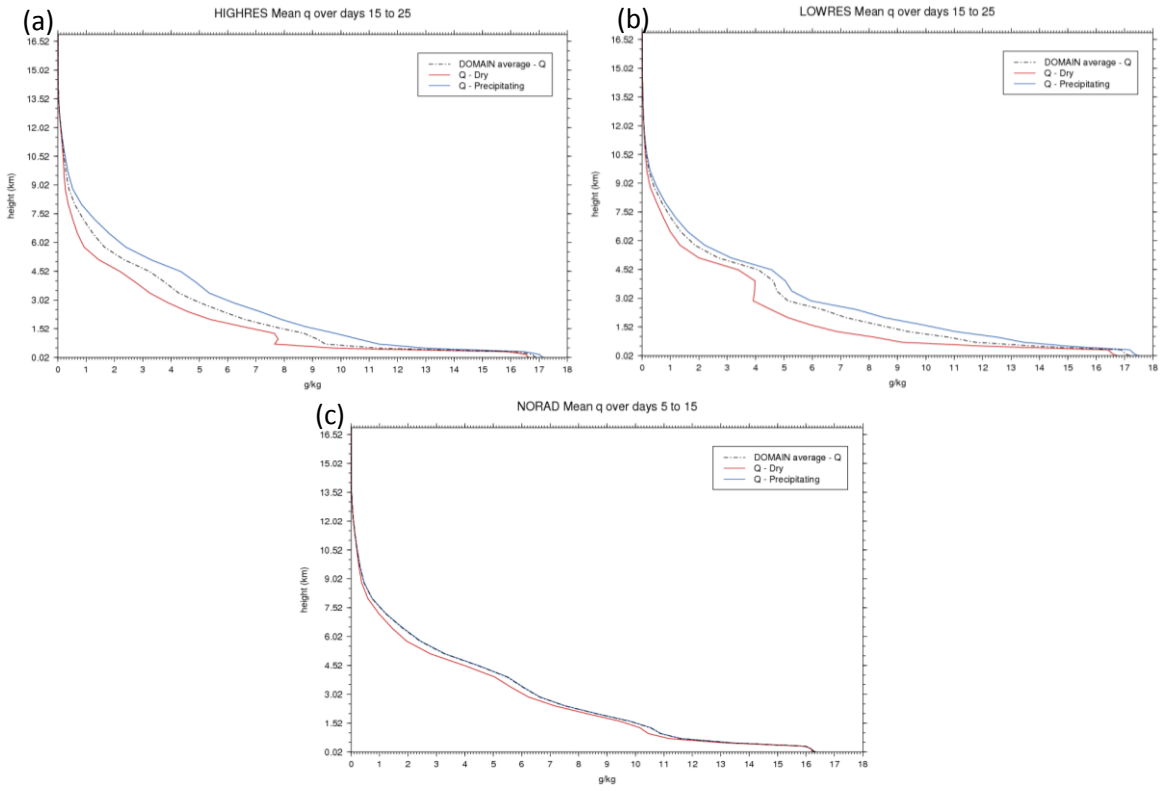

Figure 4.3 The domain-averaged specific humidity vertical profiles for a) HIGHRES days 15 to 25 mean, b) LOWRES days 15 to 25 mean, c) NORAD days 5 to 15 mean. For precipitating and dry regions.

We now consider fig. 4.1(iv) which shows the domain-averaged radiative heating profiles over days 55 to 60 of HIGHRES when the domain is in equilibrium (see Chapter 3). Aggregation is observed to be taking place in band like structures running from east to west as observed in figure 3.2. The LW cooling in the dry regions is observed to increase significantly from -5Kday^{-1} on day 25 to -7.5Kday^{-1} when the domain without the convective aggregated clusters becomes drier, as indicated by the RH profile in fig. 3.10(a). What needs to be investigated is whether or not there is boundary layer capped cloud occurring in the dry

regions, as the SW heating profile would indicate that there is with net warming at this level in the HIGHRES experiment.

c) Cloud QCL and QCF content

This section investigates the amount of cloud liquid water content (QCL) (gkg^{-1}) and the amount of cloud frozen ice (QCF) (gkg^{-1}) there is within the precipitating and dry regions of the domain. It is important to understand these contents as they tie in the link with large-scale dynamics and radiation from the previously discussed heating profiles.

In the previous section 4.1(b) it was discussed that the peak in SW radiation is found at the peak in highest proportion of ice cloud. In figure 4.5 it can be seen that the peak in QCF for the HIGHRES experiment ranges from 7.5km at day 10, to 10km by day 25. The SW peaks are observed to be at least a kilometre higher than these peaks in figure 4.1c by day 25, and this may be due to the optical thickness of the cloud. The LOWRES peak in QCF occurs at 9km at day 10, and decreases to 7.5km by day 25. The SW heating peaks (fig. 4.2) corresponds well to the peaks in QCF for the LOWRES experiment.

Figure 4.4 introduces the NORAD plots of QCL and QCF for day 10 (fig4.3a) and for day 15 (fig. 4.4b). The plots indicate that the dominant feature of the clouds within the domain is QCF content, with only small concentrations of QCL and a peak at the melting point of water (273.15K) at 4.5km. This peak in QCL may be due the effect of ice melting at this point, creating a so called bright band.

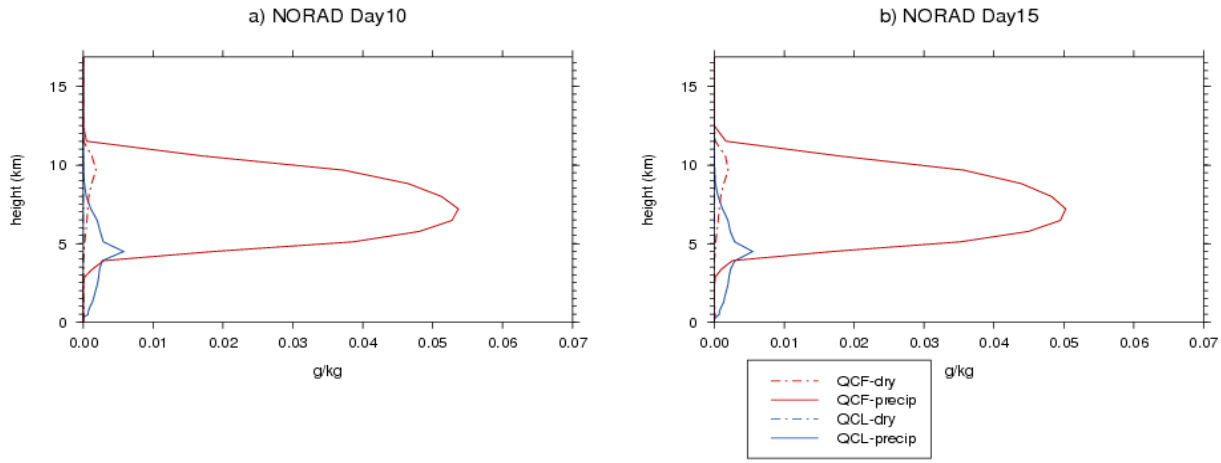

Figure 4.4 Vertical profiles of domain-averaged QCF and QCL content for the NORAD experiment, where for each day, the averages have been calculated for precipitating regions $\geq 0.001 mmhr^{-1}$, and for dry regions.

Comparing figure 4.4 with fig. 4.5(a), (c), (e), and (g) it is clear to see that in HIGHRES the QCF and QCL content is observed to grow over the duration from days 10 to 30 as the aggregation starts to develop. It could be speculated that the NORAD does not produce large-scale aggregation although it is difficult to be definitive without further days available. Certainly the QCF is observed to decrease from days 10 to 15. Within fig.4.3(a) and (b) it is clear to see that there are some traces of high level QCF in the upper troposphere with the peak at 10km in height perhaps indicating some ice clouds. However there is little or insignificant levels of QCF observed in the dry regions, and no QCL around the boundary layer in the dry regions. This indicates that something else must be causing the strong LW cooling observed in the heating profiles in figures 4.1 and 4.2.

The LOWRES plots in figure 4.5(b), (d), (f), and (h) show much less QCF and QCL content as compared with the amounts observed in the HIGHRES and NORAD. For example on day 25 (fig. 4.5h) the peak in QCF is at $0.022 gkg^{-1}$, compared to $0.13 gkg^{-1}$ of QCF in the HIGHRES (fig. 4.5g).

The LOWRES plots also indicate slightly larger values of QCF and QCL in the dry regions of the domain. Notice that the values of QCL increase from day 10 to 25 around the boundary layer. Remembering also the values found in table 3, that around 58.9% of the domain has boundary layer cumulus or stratocumulus of some form over days 1 to 25 of the model run. This boundary-layer cloud would seem to provide some of the associated LW cooling observed in figures 4.2(i), (ii), and (iii).

From the heating profiles (Fig. 4.2 and 4.3) and the QCL and QCF profiles (fig. 4.5) for the HIGHRES experiment it cannot be stated why there is such strong LW cooling, and what impact this may be having on the large-scale dynamics, and the radiation. It may be due to the fact that in the dry regions it has become extremely dry.

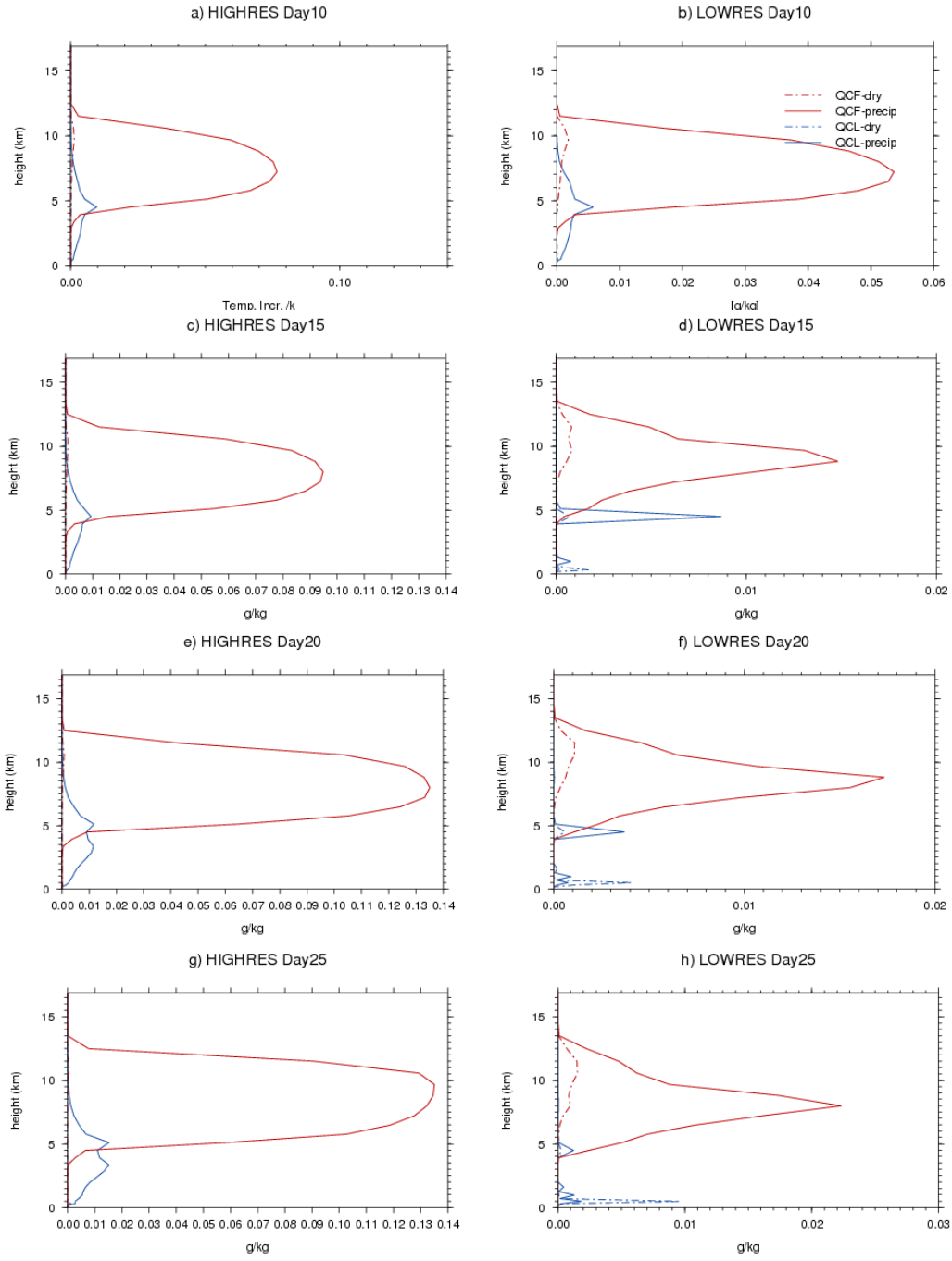

Figure 4.5 Vertical profiles of domain-averaged QCF and QCL content, where for each day, averages are calculated for precipitating regions≥0.001mmhr^{-1}, and for dry regions. Plots a), c), e), and g) are for the HIGHRES experiment, plots b), d), f) and h) are for LOWRES experiment.

Figure 4.6 is the domain-averaged QCF and QCL profiles for the HIGHRES experiment averaged over days 55 to 60 when the domain has reached equilibrium and aggregation is occurring. At day 20 to 25 aggregation is observed to be occurring, but as previously discussed in Chapter 2, this aggregation is observed to weaken, prior to starting to aggregate again on day 30. So this may not be a true representation of what is going on in the

aggregation state. So figure 4.6, when compared with 4.1(iv) showing the radiative heating rates for the same period, provides a clearer image of what is going on when aggregation is observed in equilibrium. Within the dry regions there is very little QCL and QCF if any at all indicating that there is little or no clouds in these regions affecting the LW cooling rate, and therefore it has to be due to the fact that the column has become extremely dry.

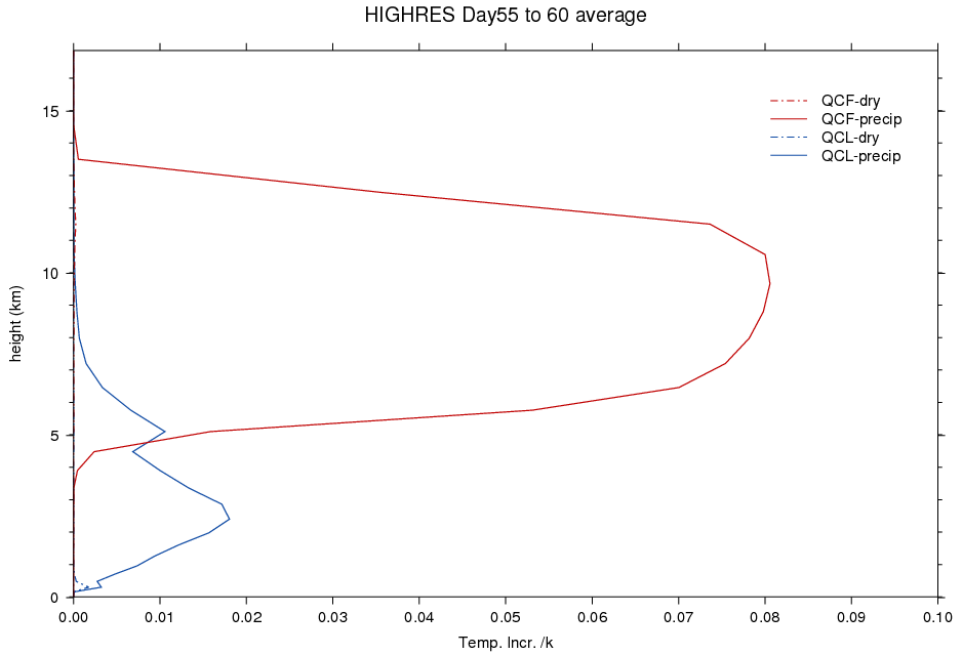

Figure 4.6 Vertical profiles of domain-averaged QCF and QCL content, where for each day, averages are calculated for precipitating regions$\geq$0.001mmhr^{-1}, and for dry regions. This plot is for the HIGHRES experiment averaged over days 55 to 60.

4.2 Investigating the LW boundary layer cooling and its impacts on circulation

There is no or very little QCL found in figure 4.5(a), (c), (e), and (g) above the boundary layer, therefore another explanation for the LW cooling is needed. Bretherton *et al.* (2005) stated that as regions start to dry out, they start to radiatively cool more strongly in the lower troposphere than the upper troposphere, as observed with HIGHRES. He goes on to state that a bottom heavy subsidence profile develops to compensate the bottom-heavy radiative cooling. The mechanism they found to feed this subsidence was by a lower to mid-tropospheric return flow from moist to dry regions which developed above the boundary layer flow from dry to moist, convecting regions. This acts to amplify the aggregation by exporting moist static energy out of the dry regions, which allows them to dry further. For more information on Bretherton *et al*'s. (2005) findings please refer to section 1.3

This section will investigate Bretherton *et al.*'s (2005) findings further to see if there is a low level circulation in the HIGHRES and LOWRES cases, and by comparing the NORAD experiment, to see if whether or not interactive radiation schemes are needed to generate this low level circulation.

a) Vertical Wind Profiles

The vertical velocity wind profiles shown in figures 4.7, 4.8 and 4.9 have been plotted for the precipitating and dry regions only, because the average values over a large domain are close to zero. In all of the figures the areas of precipitation are associated with updrafts, and dry regions are associated with subsidence. Both will contain updrafts and downdrafts, but these are averaged out in these results which show the large-scale circulation.

Figure 4.7 is the vertical velocity profile for the NORAD experiment, for days 10 and 15. The pattern is almost symmetrical between precipitating and dry regions. When comparing this with figure 3.1, which shows that almost half of the domain is precipitating, the near asymmetry is expected. By day 15 the positive vertical velocities are starting to decrease as the percentage of rainfall events increases, and it could be speculated that this would continue to decrease. This is because in figure 4.8, for the HIGHRES experiment, the percentage of precipitating events is decreasing, and the positive vertical velocities are observed to increase in time.

As just discussed in the HIGHRES case the vertical updraft velocities are observed to increase over time in the upper troposphere. This increase in the upper troposphere is due to the increase in ice as seen in figure 4.5 as the ice has a greater terminal velocity than liquid water.

The strong radiative cooling in the lower troposphere is observed in the HIGHRES case and just above the surface a subsidence profile is developing and increasing as found by Bretherton *et al.* (2005). In Bretherton *et al.*'s (2005) study, to balance this subsidence, a lower to mid-tropospheric return flow from moist to dry regions developed above the boundary layer flow from dry to moist. Within figure 4.8 it is clear to see that by continuity there must be a similar circulation occurring. This is marked by the arrows, with divergence at the top of the boundary layer, and convergence below in the precipitating regions, and the opposite in the dry regions.

The LOWRES experiment has the bottom heavy subsidence but it is perhaps more difficult to tell whether or not it has this lower circulation as discussed by Bretherton *et al.* (2005) and found here in the HIGHRES. This is because of the diagnostics previously discussed in section 4.1(b) Table 3, which show that there is cumulus and stratocumulus which will be associated with their own circulation systems within the boundary layer. However this does not mean that the continuity argument breaks down, there is another type of boundary layer motion going on as well.

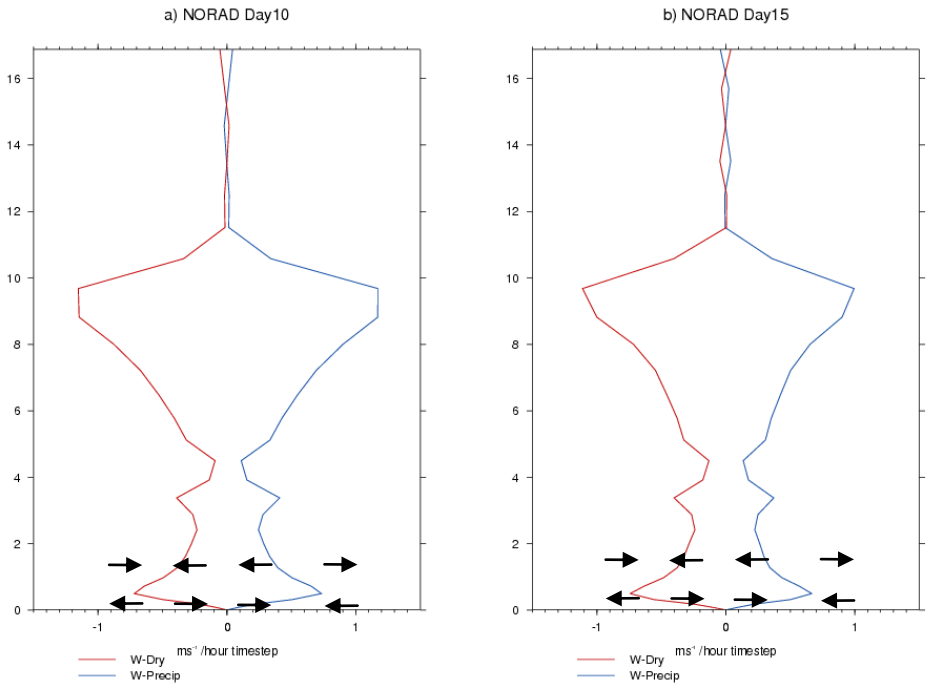

Figure 4.7 The domain-averaged vertical velocity profile for the NORAD experiment, segmented into precipitating and dry regions, a) day 10, b) day 15. Vertical height is in [km].

With a horizontally fixed net radiative heating profile the NORAD model cannot adapt to its environment. A lower circulation must be present in figure 4.7 by mass continuity as there is for the HIGHRES experiment. However it is "balanced" convective and moisture fluxes driving the circulations in the NORAD, generating disorganized convection. It can be hypothesised that interactive radiation is needed to generate the cooling in the dry region; hence a stronger circulation to counteract this imbalance.

Figure 4.9 shows the domain-averaged vertical velocity profile over days 55 to 60. It has a peak in low level subsidence to compensate the strong LW cooling observed in figure 4.1(iv). This mechanism is still acting to feed the aggregated clusters with moist static energy, hence continuing to dry the region without precipitation and feeding the aggregation.

- FIGURE 4.8 -

The domain-averaged vertical velocity profile for the HIGHRES (a, c, e) and LOWRES (b, d, f) experiments, segmented into precipitating and dry regions, for days 15,20 and 25. Arrows have been added to represent the low level convergence and divergence.

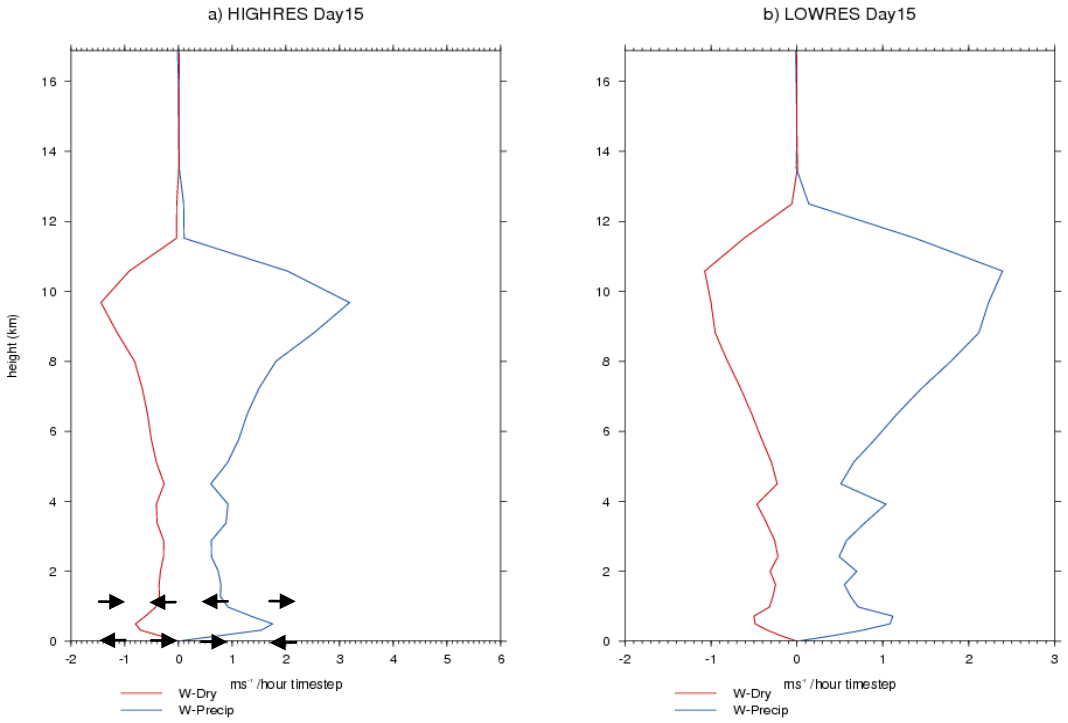

Figure 4.8 a) HIGHRES, b) LOWRES, day 15 vertical velocity profiles.

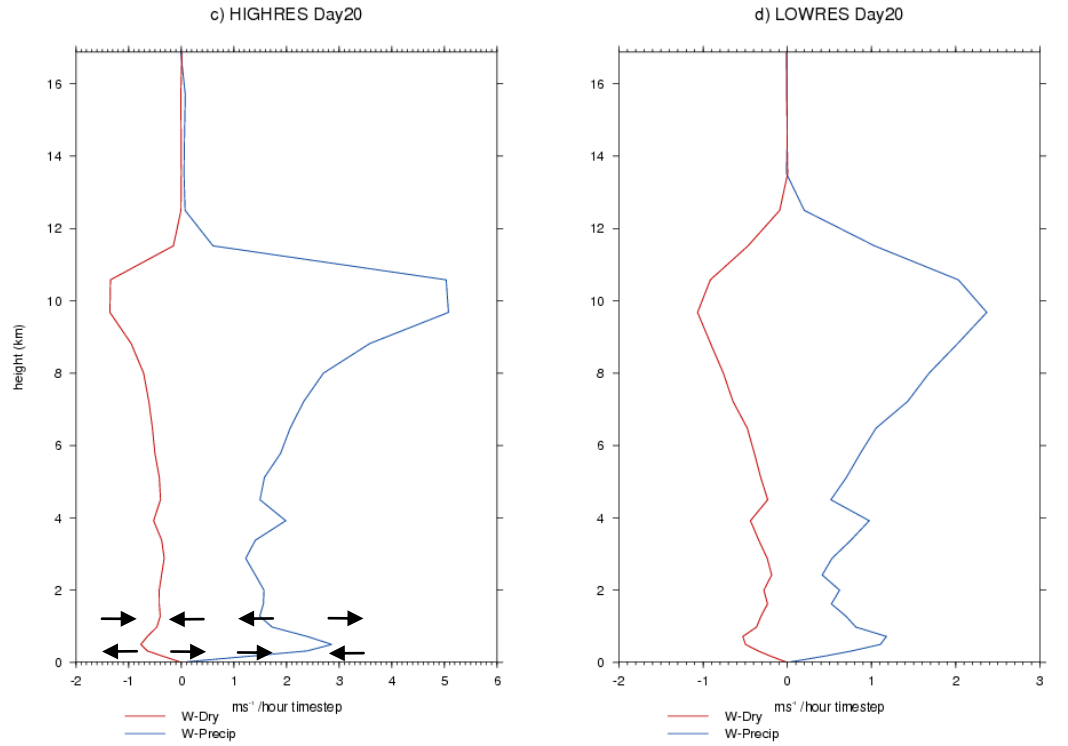

Figure 4.8 c) HIGHRES, d) LOWRES, day 20 vertical velocity profiles.

- FIGURE 4.8 -

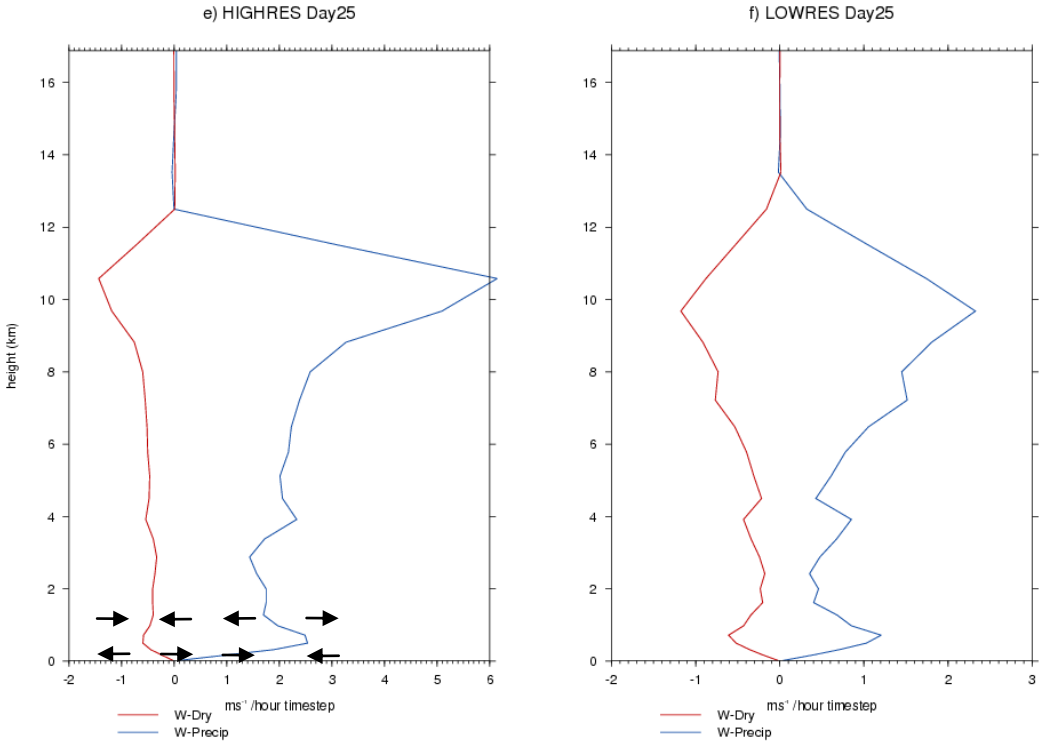

Figure 4.8 e) HIGHRES, f) LOWRES day 25 vertical velocity profiles

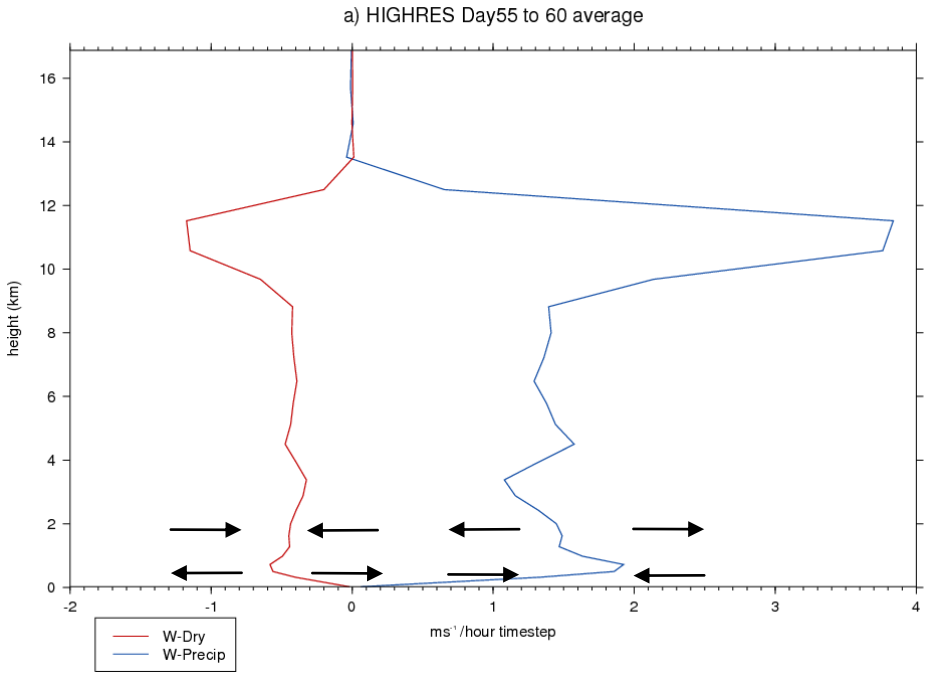

Figure 4.9 The domain-averaged vertical velocity profile for the HIGHRES experiment sorted into precipitating and dry regions, for averaged over days 55 to 60 inclusive. Arrows represent the low level convergence and divergence.

b) u and v increments to investigate the low level circulation in the HIGHRES experiment

The u and v increments have been plotted to investigate whether or not there is any coherence between the vertical profiles of these increments and the low-level circulation as deduced earlier by mass continuity in the precipitating and dry regions.

In figures 4.10 and 4.11 the domain-averaged a) u increments and b) v increments are plotted for 3 different processes; Boundary layer and large-scale cloud, convection, and advection for dry and precipitating regions.

Figure 4.10 for HIGHRES is for day 25, when just prior to when the aggregation is observed to dissipate slightly before it rebuilds at day 30. In the wet regions the advection terms acting to produce a circulation, with positive u increments below 1km and negative just above, perhaps associated with some low level convergence and upper level divergence. The convection increments mimics this but with much smaller values. The boundary layer winds act the opposite way to the advection term, the friction within the boundary layer acts to reduce wind speed, so if some low-level circulation process is acting to increase low-level winds, the boundary layer will tend to act against this, and offset the strength of this. This pattern also emerges in day 55 to 60 average (fig. 4.11); however the values have increased in strength, and switched sign at the bottom and top of this low level circulation. This sign change in a cyclic domain is deemed not to be important, what is important is that there is a vertical dipole in the increments.

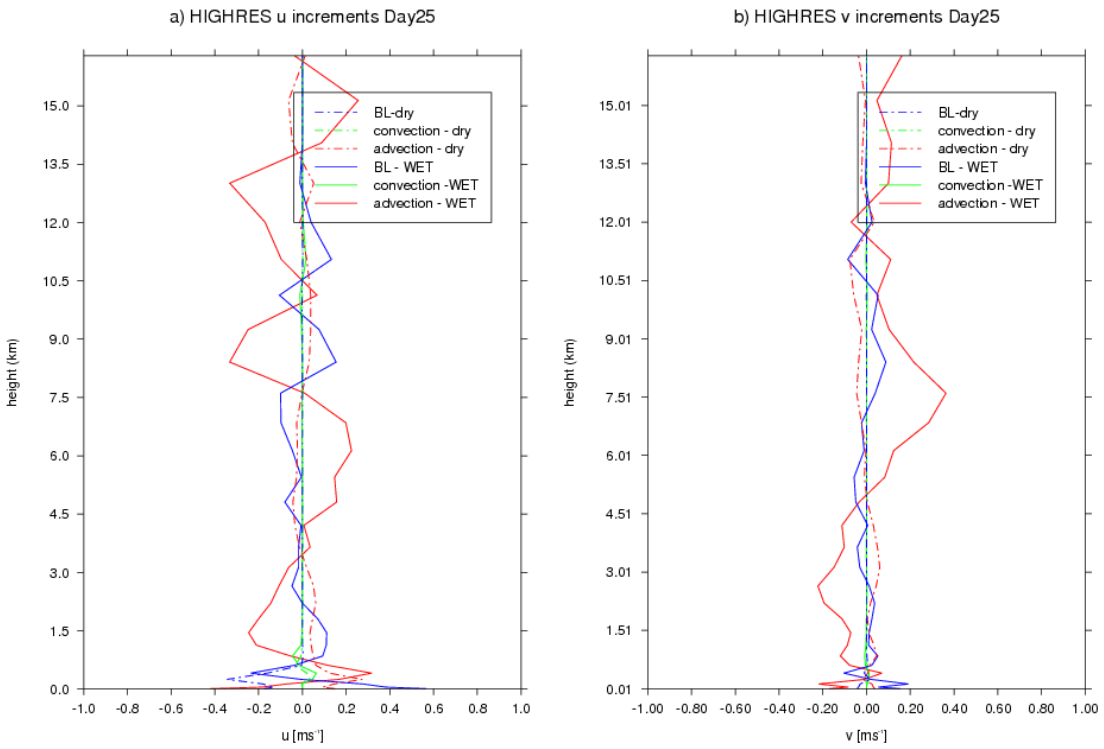

Figure 4.10 The domain-averaged a) u increments and b) v increments for the HIGHRES model, where the units are in ms^{-1} per day timestep for day 25. Averages are made for both precipitating and dry regions.

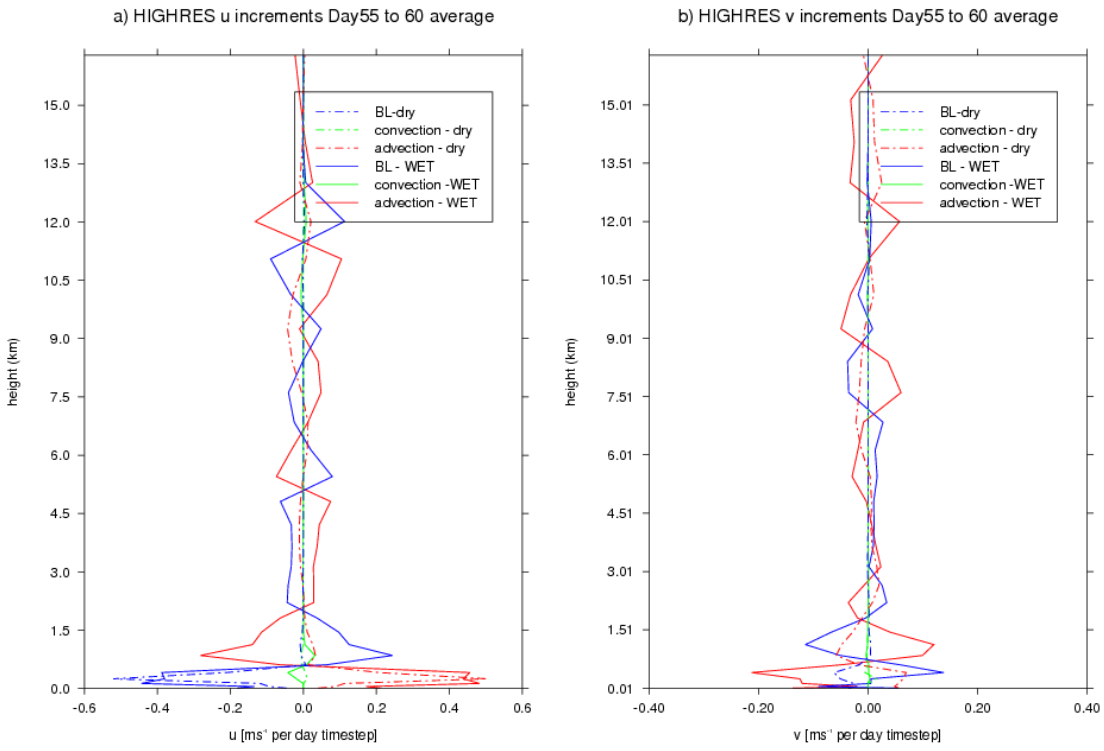

Figure 4.11 The domain averaged a) u increments and b) v increments for the HIGHRES model, where the units are in ms^{-1} per day timestep for the average over days 55 to 60 inclusive. For either precipitating or dry regions.

c) Specific humidity increments to investigate the role of the low level flow in HIGHRES

All of the q increments shown in figures 4.12 and 4.13 act to balance (fig. 4.14) each other and describe the circulation of moisture around the domain. These plots have been created to investigate what moisture is being transported where in the dry and precipitating regions in the HIGHRES experiment. Alongside the u and v increments that this low level circulation is occurring.

Within both figures 4.12 and 4.13 the advection increments are acting to remove moisture from the dry regions, which is then being advected into the wet regions at low levels. This is as seen in vertical velocity profiles and figures 4.10 and 4.11, indicating that the moisture is transported up a few hundred metres; the peak is observed to be at the same level of convective updraft at days 25 (fig. 4.7e) and days 55 to 60 (fig. 4.8). Above this level, moisture transport is observed to decrease with the associated change in u and v components in the advection and boundary layer and large scale cloud terms, i.e. divergence aloft of the convergence in the low level circulation.

The total q increments in figure 4.14 is the sum of all the components used to plot figures 4.12 and 4.13, for (fig. 4.14a) days 10 to 15 average, and for (fig. 4.14b) days 55 to 60 average. In figure 4.14(a) the wet columns are staying almost constant throughout the period of days 10 to 15, while the dry columns are getting drier. From this it can be concluded that the hypothesis that there is a circulation between the wet and dry regions it cannot be simply explained by a low level circulation system, there are more complex interactions taking place between the dry and moist regions. But this is easily considered as the domain as a whole is becoming progressively drier as the HIGHRES experiment reaches equilibrium.

In the later stages of the HIGHRES experiment there are time cycles of differing amounts of aggregation occurring, as observed in Chapter 3 (figs. 3.1, 3.2, 3.6, 3.9). This investigation has not looked at this, so therefore it is difficult to decipher what is happening in figure 4.14(b), with the drying below 4km in the moist columns and the moistening in the dry columns below 3km.

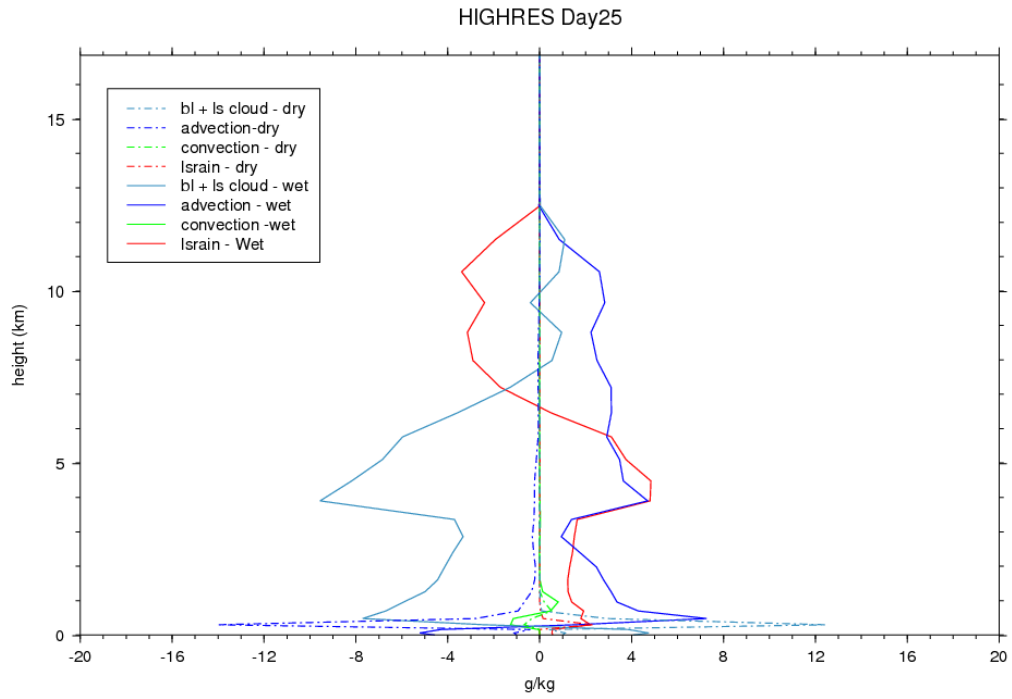

Figure 4.12 The domain-averaged specific humidity increments for HIGHRES day 25, where the increments include boundary layer and large scale cloud, advection, convection, and large scale rain. The units are gkg^{-1} per day timestep.

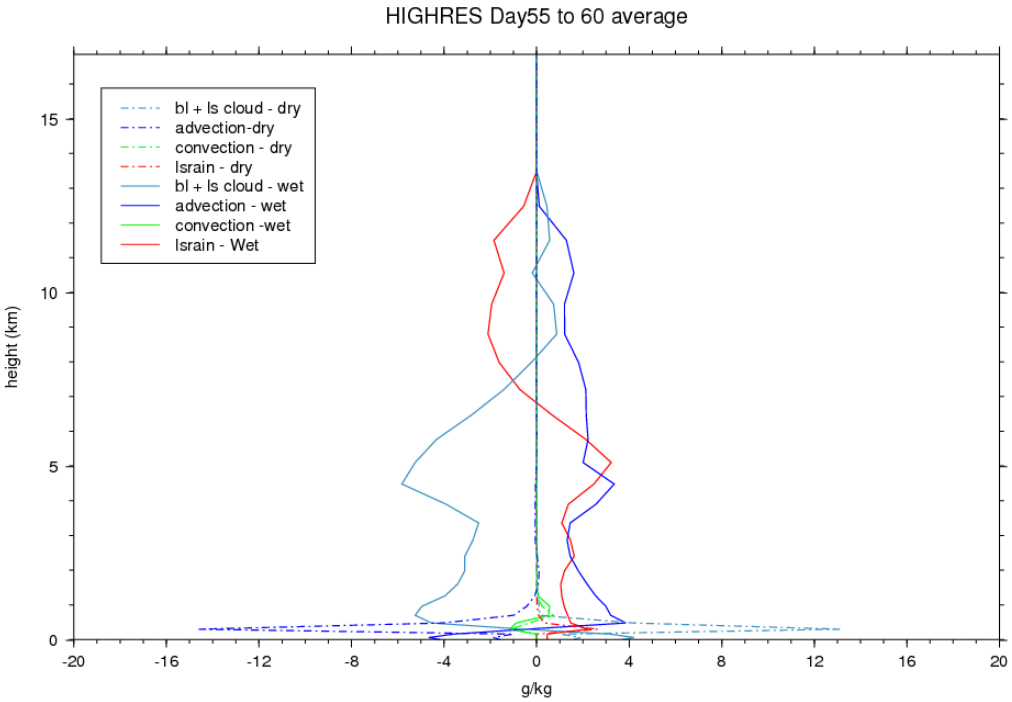

Figure 4.13 The domain-averaged specific humidity increments for HIGHRES day 55-60 average, where the increments include boundary layer and large scale cloud, advection, convection, and large scale rain. The units are gkg^{-1} per day timestep.

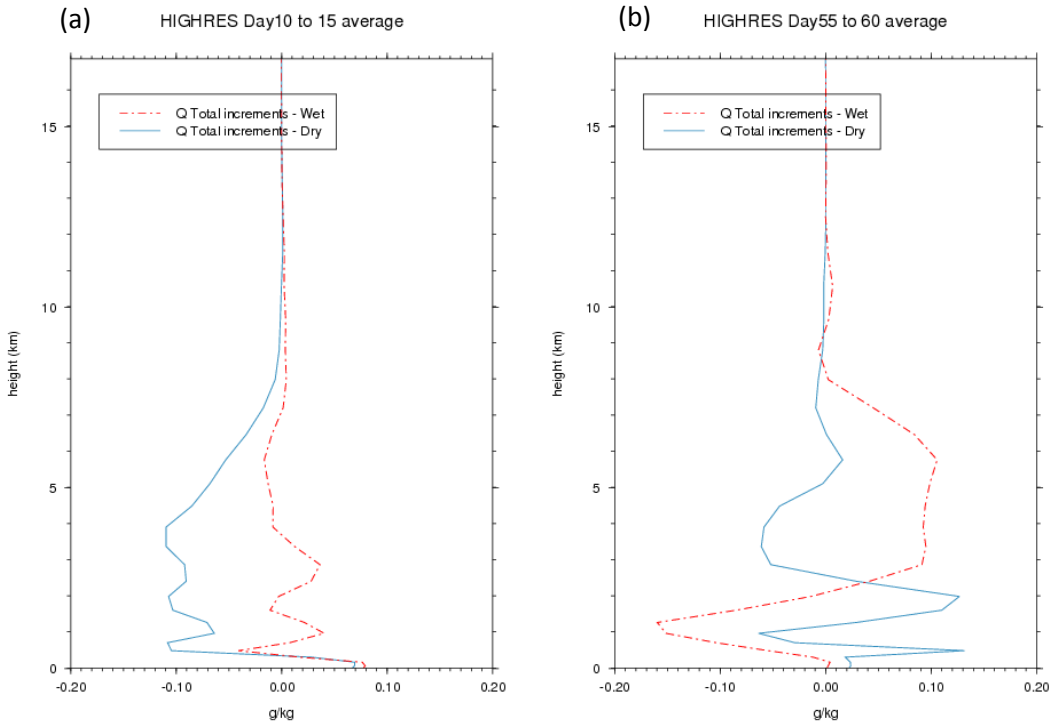

Figure 4.14 The domain-averaged total specific humidity increment for HIGHRES days (a) 10 to 15, and (b) 55 to 60 mean, where the increments include boundary layer and large scale cloud, advection, convection, and large scale rain. The units are gkg^{-1} per day timestep.

Chapter 5 - Conclusion and Summaries

5.1 Summary of Results

This reports main focus of this investigation has been heavily weighted towards the investigation on the effects the interactive radiation scheme has on the convective and large-scale dynamics, and its function in the creation and ability to allow convective aggregation to take place and continue. But firstly it was important to consider if self aggregation was occurring, by investigating whether or not Radiative Convective Equilibrium had been reached. This was achieved using three idealized model experiments, HIGHRES, LOWRES, and NORAD from the UK Met office Unified Model (4km, 40km, and 4km runs).

5.1.1 Results (i) - Analysis of Self-aggregation

In Chapter 3, it was first hypothesised that an interactive radiation scheme, as prescribed in the HIGHRES and LOWRES experiments is a crucial element for self-aggregation to occur. All three experiments started off with similar values of approximately 40% of the domain with precipitating grid points greater than $0.001 mmday^{-1}$. The HIGHRES and LOWRES experiments indicated a trend to decrease in time. The HIGHRES experiment dropped as low as 18% of the domain by day 60. The NORAD experiment showed a clear indication of an increase from 41.7% to 53%.

To test the hypothesis true, firstly, the analysis of the time evolution of domain-averaged OLR plots for the HIGHRES and LOWRES experiments was invetigated. It was concluded that aggregation was occurring in the HIGHRES by day 50 in the form of bands (perhaps squall line structures) from left to right across the domain, with the OLR increasing in the rest of the domain agreeing with previous studies (e.g Tompkins and Craig, 1998, Bretherton *et al.*, 2005, Stephens *et al.*, 2007, Nolan *et al.*, 2007). In the LOWRES it was difficult to conclude if aggregation was occurring from the OLR plots, but large areas of cloud clusters were observed.

To test the hypothesis further analysis of the equilibrium state was performed, by investigating QRAD and THF, FMSE as defined by Bretherton *et al.* (2005), equivalent potential temperature, and relative humidity.

The HIGHRES experiment has been able to prove the hypothesis correct in this case, by reaching an equilibrium state by day 50, agreeing with the findings of Tompkins and Craig

(1998b). This was observed in the QRAD and THF (fig. 3.6a, page 25) becoming stable and the difference becoming negligible. The daily precipitation rate (fig. 3.6b, page 25) indicates a change in the scales of aggregation size when in equilibrium, on a 3 to 5 day timescales. The general trend in FMSE (fig. 3.9a, page 31) matched the QRAD and THF balance trends well, reaching equilibrium at day 50. The THETA_E profile is also a key indicator that the model has reached equilibrium; the domain had a large cold pool across the middle of the domain, which matched the high OLR in fig. 3.2(g). The RH profile indicated tropospheric drying by day 60, matching what was found by Bretherton *et al.* (2005) at equilibrium.

The LOWRES experiment results proved it difficult as to whether or not an equilibrium state was satisfied. The QRAD and THF plots indicate an equilibrium state reached by day 25 with the lines becoming stable and the difference negligible. The daily precipitation rate however shows an increasing trend, but without large fluctuations which were observed in the HIGHRES experiment. The FMSE plot disagrees with the QRAD and THF plot, with no significant difference between the two, as it appears to be rising at day 30. The THETA_E profile maybe similar to that of the HIGHRES case, just on a larger domain, but once again does not clarify equilibrium. The RH plot indicated a drying of the upper tropopause by day 30 of the model run, unlike the HIGHRES experiment. In summary the LOWRES experiment has not reached equilibrium by the end of the model run, but large-scale aggregation is starting to take place.

The NORAD experiment can be concluded that an equilibrium state is not reached, through the QRAD and THF plot and the FMSE plot. The radiative cooling of the atmosphere (QRAD) is fixed in space and time, but the THF is observed to drop off by day 7, which ties together well with the increasing trend in FMSE. No stability in any of the plots is observed. There is no self-aggregation by at least day 15 of the model run.

5.1.2 Results (ii) - Investigation into the radiation interaction effects, and fluxes generated

In Chapter 4 it was hypothesised that an interactive radiation scheme is needed to generate a low-level circulation, similar to Bretherton et al.'s (2005) findings. Where a low level subsidence takes place due to the strong longwave radiative cooling at the surface in the dry regions of the model domain. To drive this subsidence, a return flow from moist to dry regions in the lower troposphere, develops above the boundary layer flow from dry to moist

regions. Which Bretherton *et al.* (2005) argued it acted to amplify self-aggregation by removing moist static energy from the dry regions.

This hypothesis was generated by an investigation into the radiative heating rates, the QCL and QCF vertical quantities, and vertical wind profiles, in precipitating and dry regions

For all three experiments there is strong LW cooling associated either in or on top of the boundary layer, with a maximum cooling rate of $-5Kday^{-1}$ in the HIGHRES case on the days 55 to 60 average. With investigations into the boundary layer parameterization diagnostics it was found that for the LOWRES experiment 50.89% of the domain has boundary layer capping cloud over the first 25 days of the model run. Therefore the LW cooling in the LOWRES was deemed to be due to low boundary layer cloud and high specific humidity content in the dry regions. The QCL values for the HIGHRES experiment indicated little or no cloud associated at this level in the dry regions of the domain, and the q plot (fig. 4.3a) indicates very dry air at the level of observed strong LW cooling. The heating rate for the NORAD experiment is the 3 to 5 day average taken from the HIGHRES model, and this is not able to change to its respective environment; but it still had a LW cooling of $-3Kday^{-1}$ fixed throughout the model run time.

The vertical wind profiles for all three experiments indicate that by mass continuity there must be a low level circulation. But the circulation is only thought to have an effect in the HIGHRES and LOWRES experiments on the aggregation, this is due to the fact that the larger the LW cooling, a larger flux rate occurs to correct this imbalance by mass continuity.

To test the hypothesis further, investigations were concentrated on the HIGHRES experiment. The advection and boundary layer increments are found to provide an inclination of a circulation taking place. The 55 to 60 day running average indicates that there was a vertical dipole in the u and v increments. The specific humidity increments suggest of a low level circulation, but from the total specific humidity increments it has been concluded that although there is a low level circulation taking place, there are far more complicated interactions taking place between the moist and the dry columns.

5.1.3 Conclusion

In conclusion the first hypothesis tested in Chapter 3 is in conclusive, due to the fact that the LOWRES experiment was producing imbalanced results in the case of it being in equilibrium

or not. The HIGHRES reaches RCE and produces large-scale aggregation, and the NORAD experiment does not reach RCE for self-organized-aggregation to occur.

In the case of the low level circulations between the dry and moist regions, it can be confirmed a low level circulation is taking place, but it is not the only mechanism interacting with the aggregated clusters. But it is confirming Bretherton *et al.*'s (2005) findings.

5.2 Project Limitations

The main limitation of this work is a lack of model run time data for the LOWRES and NORAD experiments. It is difficult to test the hypotheses as to whether or not if they reach an equilibrium state with established associated aggregated clusters. In the past studies have shown some form of convective clusters in fixed radiative forcing studies.

5.3 Future Work

Within the first days of all three model experiments, random convection in space in time was observed. However to investigate further the first phase or state of random convection in space and time as stated by Emanuel and Khairoutdinov (2010), it would be interesting how to define this state with parameters.

The difference between the QRAD and the THF line plots at equilibrium would represent the role of the sea as the storage component (G) of the of the radiation budget equation. If the QRAD is greater than the THF for long periods of time, it could be implied that the SST would be observed to cool. Emanuel and Khairoutdinov (2010) observed this with an interactive SST, it could be suggested that this is a mechanism to break up the organization in the end. It would be an interesting investigation to see what impact this would have, on aggregation and the propagation of clusters across the domain.

In the HIGHRES experiment a sharp drop in QRAD was observed on day 23, which may of led to the aggregation which started to occur prior to day 30 to dissipate introducing a minima in daily precipitation associated with weaker stratiform and broken clusters of convection. It could be a mechanism to break up the aggregation when the model is in equilibrium.

In all three experiments an increase in RH was observed at the tropopause level by the last day of the model run. Further investigation could look into whether or not this is raising the level of the tropopause or even penetrating the stratosphere which may have an impact on the large scale circulation.

Further analysis is needed into the interactive mechanisms with the moist and dry columns, the feeding mechanisms, to figure out what is happening in the total q increments profile on days 10 to 15, and 55 to 60.

References

Arakawa, A., W.H. Schubert, 1974: Interaction of a cumulus cloud ensemble with the large scale environment part I. *Journal of the Atmos. Sci.* **31**, 674-701.

Bretherton, C.S., P.N. Blossey, M. Khairoutdinov, 2005: An Energy-balance analysis of deep convective self-aggregation above uniform SST. *Journal of the Atmos. Sci.* **62**, 4273-4292.

Bryers, H.R., Braham, Jr., 1948: Thunderstorm structure and circulation. *J. Meteor.* **5**, 71-86.

Cetrone, J., and R.A. Houze, 2009: Anvil clouds of tropical mesoscale convective systems in monsoon regions. *Quarterly Journal Royal Meteorological Society*. **135**, 305-317.

Davies, T. M.J.P Cullen, A.J. Malcolm, M.H. Mawson, A. Staniforth, A.A. White, and N. Wood, 2005: A new dynamical core for the Met Office's global and regional modelling of the atmosphere. *Q.J.R. Meteorol. Soc.* **131**, 1759-1782.

ECMWF, 2007: Parameterization [online]. Available at: http://www.ecmwf.int/products/forecasts/forecasts/guide/Parametrization.html [1/06/2010]

Edwards, J., and A. Slingo, 1996: Studies with a flexible new radiation code. Part I: Choosing a configuration for a large scale-model. *Q.J.R. Meteorol. Soc.* **122**, 689-719.

Emanuel, K.A., 1994: *Atmospheric Convection.* 1st Edn. Oxford University Press, 580 pp.

Emanuel, K.A., and M.F. Khairoutdinov, 2010: Aggregated convection and the regulation of tropical climate. Preprints, *29th conference on Hurricanes and Tropical Meteorology*, Tucson, AZ, Amer. Meteor. Soc., P2.69.
[Available online at http://ams.confex.com/ams/pdfpapers/168418.pdf.]

Grabowski, W.W., J.C. Petch, 2009: Deep Convective Clouds. *Clouds in the perturbed climate*, J. Heintzenberg and R.J. Charlson, Eds. , The MIT Press, 197-216.

Gregory, D., P.R. Rowntree, 1990: A mass flux convection scheme with representation of cloud ensemble characteristics and stability dependent closure. *Mon. Wea. Rev.* **118:** 1483-1506.

Hastenrath, S., 1985: *Climate and Circulation of the Tropics.* D.Reidel Publishing Company, Holland. pp 455

Houze, R.A. Jr., 1993: *Cloud Dynamics.* Academic Press, Inc., London. pp 573
LeMone, M.A., E.J Zipser, and S.B. Trier, 1998: The role of environmental shear and CAPE in determining the structure and evolution of mesoscale convective systems during TOGA COARE, *J. Atmos. Sci.* **55**, 3493-3518.

Lee, M.-I., I.-S. Kang, J.-K. Kim, and B. E. Mapes, 2001: Influence of cloud-radiation interaction on simulating tropical Intraseasonal oscillation with an atmospheric general circulation model. *J. Geophys. Res.,* **106** (D13), 14 219–14 233.

Lee, M.-I., I.-S. Kang, J.-K. Kim, and B. E. Mapes, 2003: Impacts of cumulus convection

parameterization on aqua-planet AGCM simulations of tropical intraseasonal variability. *J. Meteor. Soc. Japan*, **81**, 963–992.

Lock, A.P., A.R. Brown, M.R. Bush, G.M. Martin, R.N.B. Smith, 2000: A new boundary layer mixing scheme. Part I: Scheme description and single-column model tests. *Mon. Wea. Rev.* **128**, 3187-3199.

Madden, R.A. and P.R. Julian, 1972: Description of global-scale circulation cells in the tropics with a 40-50 day period. *J. Atmos. Sci*., **29**, 1109 – 1123.

Madden, R.A. and P.R. Julian, 1994: Observations of the 40-50 day tropical oscillation – a review. *Mon. Wea. Rev*., **122**, 814-837.

Malkus, J.S., 1954: Some results of a trade-cumulus cloud investigation. *J. Meteor.* **11**, 220-237.

Maloney, E. D., and D. L. Hartmann, 2001: The sensitivity of intraseasonal variability in the NCAR CCM3 to changes in convective parameterization. *J. Climate*, **14**, 2015–2034.

Maloney, E. D., 2002: An intraseasonal oscillation composite life cycle in the NCAR CCM3.6 with modified convection. *J. Climate*, **15**, 964–982.

Mather, J. H., S. A. McFarlane, M. A. Miller, and K. L. Johnson, 2007: Cloud properties and associated radiative heating rates in the tropical western Pacific, *J. Geophys. Res*., **112**, 19pp.

McPhaden, M.J., 1999: Genesis and evolution of the 1997-98 El Nino. *Science*, **283**, 950-954.

Moncrieff, M.W., 2004: Analytic Representation of the Large-Scale Organization of Tropical Convection. *J. of the Atmos. Sci.* **61**, 1521-1538.

Nakazawa, N., 1988: Tropical Super Clusters within Intraseasonal Variations over the Western Pacific. *J. of the Met. Soc. of Japan*. **66**, 823-838.

Nolan, D.S., E.D. Rappin, K.A. Emanuel, 2007: Tropical Cyclogensis sensitivity to environmental parameters in radiative-convective equilibrium. *Q.J.R. Meteorol. Soc.* **133**. 2085-2107.

Roberts, N.M., 2003: Stage 2 report form the storm-scale numerical modelling project. Technical report 407, MetOffice R&D, [Available online at

Slingo, J. M., and Coauthors, 1996: Intraseasonal oscillations in 15 atmospheric general circulation models: Results from an AMIP diagnostic subproject. *Climate Dyn.*, **12**, 325–357.

Smagorinsky, J., 1963: General Circulation experiments with the primitive equations. Part I: The basic experiment. *Mon. Wea. Rev.*, **91**, 99-164.

Srinivasan, J., and Smith, G.L., 1996: The role of heat fluxes and moist static energy in Tropical Convergence zones. *Mon. Wea. Rev.*, **124**, 2089-2099.

Stephens, G.L., S.V.D. Heever, L.Pakula, 2008: Radiative-Convective Feedbacks in Idealized States of Radiative-Convective Equilbrium. *Journal of Atmos. Sci.* **65**, 3899-3916.

Tao, W.K., S. Lang, J. Simpson, C.H. Sui, B. Ferrier, and M.D. Chou, 1996: Mechanisms of Cloud-Radiation Interaction in the Tropics and Midlatitiudes. *J. Atmos. Sci.* **53**, 2624-2651.

Tompkins, A.M., and G.C. Craig, 1998a: Radiative-Convective equilibrium in a three-dimensional cloud-ensemble model. *Q.J.R. Meteorol. Soc.* **124**, 2073-2097.

Tomkins, A.M., and G.C. Craig, 1998b: Time-scales of adjustment to radiative-convective equilibrium in the tropical atmosphere. *Q. J. R. Meteorol. Soc.* **124**, 2693-2713.

Tompkins, A.M., 2001a: Organization of tropical convection in low wind shears: The role of water vapor. *J. Atmos. Sci.* **58**, 529-545.

Tompkins, A.M., 2001b: Organization of tropical convection in low vertical wind shears: The role of cold pools. *J. Atmos. Sci.* **58**, 1650-1672.

Waliser, D., K. Sperber, H. Hendon, D. Kim, E. Maloney, M. Wheeler, K. Weickmann, J. Gottschalck, W. Higgins, D. Leger, M. Moncrieff, S. Schubert, W. Stern, F. Vitart, B. Wang, W. Wang, and S. Woolnough, 2009: MJO Simulation Diagnostics. *Journal of Climate.* **22**. 3006-3030.

Wang, W. Q., and M. E. Schlesinger, 1999: The dependence on convection parameterization of the tropical intraseasonal oscillation simulated by the UIUC 11-layer atmospheric GCM. *J. Climate*, **12**, 1423–1457.

Wilson D.R., and S.P. Ballard, 1999: A microphysically based precipitation scheme for the UK Meteorological Office Unified Model. *Q.J.R Meteorol. Soc.* **125**, 1607-1636.

Wu, X., and X. Li, 2008: A review of cloud-resolving model studies of convective processes. *Advances in Atmospheric Sciences.* **25**, 202-212.

Yuan, J., and R.A. Houze, 2010: Global Variability of Mesoscale Convective System Anvil Structure From A-Train Satellite Data. *Journal of Climate.* **Submitted.** [Available online at http://www.atmos.washington.edu/~gcg/MG/PDFs/JCLIM10_YuanHouze_GlobalVariability REVISED.pdf]

Zipser, E.J., 2003: Tropical Precipitating Systems. *Handbook of weather, climate, and water,* T.D. Potter and B.R. Colman, Eds., Wiley-Interscience, 621-632